frontiers | Frontiers in Earth Science

TYPE Original Research
PUBLISHED 25 August 2022
DOI 10.3389/feart.2022.963351

OPEN ACCESS

EDITED BY
Kit Lai,
Fortescue Metals Group, Australia

REVIEWED BY
Shiwei Wang,
Hefei University of Technology, China
Jing Chen,
Qinghai Normal University, China

*CORRESPONDENCE
Chulin Xia,
xiachulin@163.com

SPECIALTY SECTION
This article was submitted to Geochemistry, a section of the journal Frontiers in Earth Science

RECEIVED 07 June 2022
ACCEPTED 14 July 2022
PUBLISHED 25 August 2022

CITATION
Zhang W, Xia C, Zhen S, Quan C, Du Y and Han Z (2022), Geochronology and geochemistry of Late Triassic granitoids in Harizha Cu polymetallic deposit (East Kunlun Orogen) and their metallogenic constraints.
Front. Earth Sci. 10:963351.
doi: 10.3389/feart.2022.963351

Geochronology and geochemistry of Late Triassic granitoids in Harizha Cu polymetallic deposit (East Kunlun Orogen) and their metallogenic constraints

Wenzhao Zhang[1], Chulin Xia[1,2]*, Shikun Zhen[1], Chang'en Quan[1], Yu Du[1] and Zhihong Han[1]

[1]Qinghai University, Xining, Qinghai, China, [2]Key Laboratory of Cenozoic Resource and Environment in North Margin of the Tibetan Plateau, Xining, Qinghai, China

The large Harizha copper (Cu) polymetallic deposit is located in the eastern section of East Kunlun Orogen. The ore-related lithologies include mainly the granodiorite, monzogranite, and their porphyries. Zircon U-Pb dating of the ore-bearing granodiorite porphyry and granite porphyry yielded Late Triassic age of 217 Ma. The rocks are characterized by being rich in SiO_2 (68.44–78.13 wt%) and high alkali (4.03–8.33 wt%) and peraluminous (A/CNK = 1.02–1.68). In general, the granite samples are peraluminous and high-K calc-alkaline. The rocks are significantly enriched in light rare earth elements (LREE), large ion lithophile elements (e.g., K, Rb, Ba) and other incompatible elements (e.g., U, Th), but are depleted in heavy rare earth elements (HREEs), with weakly negative Eu and Ce anomalies, resembling I-S transitional granite. The zircons have ε_{Hf} (t) = -8 to -4, and the corresponding zircon two-stage Hf model age (T_{DM2}) from 1.5 to 1.8 Ga. We speculated that the ore-forming materials in the mining area were mainly from partial remelting of crustal materials, and that the tectonic regime was post-collisional extension.

KEYWORDS

granodiorite-porphyry, zircon U-Pb dating, geochemistry, the Harizha Cu polymetallic deposit, East Kunlun metallogenic belt

1 Introduction

Porphyry copper deposit is the world's most important copper deposit type, and is characterized by being large-scale, low-grade (Zhai et al., 2011; Park et al., 2021). Porphyry copper deposits in the region were mainly formed in the late Mesozoic (Yanshanian) and Cenozoic (Himalayan), when the Indian plate subducted northward and collided with Eurasia, resulting in multiphase tectonism and magmatism that provided favorable metallogenic conditions (Tang et al., 2010; Liu et al., 2019).

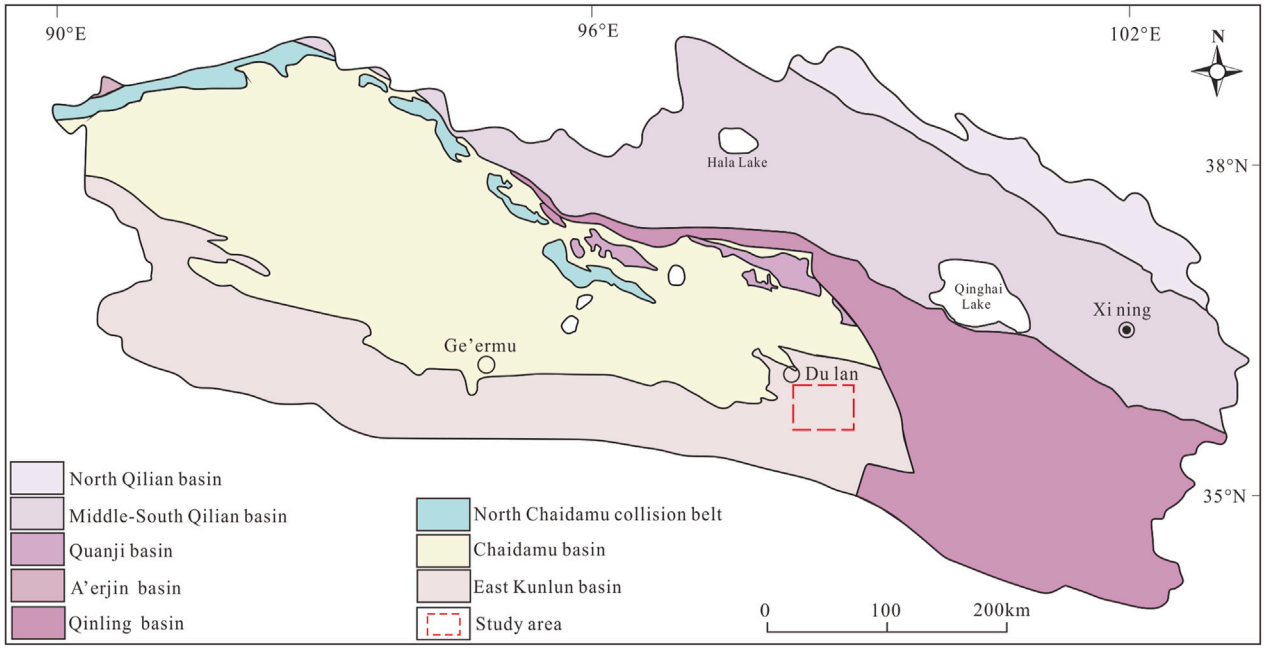

FIGURE 1
Geotectonic location map of the eastern East Kunlun Orogen (modified after Yang et al., 2017).

Typical porphyry Cu deposits include the Aktogai in Kazakhstan (Chen et al., 2010), the Escondida porphyry copper deposit and Collahuasi porphyry Cu-Mo in northern Chile (Urqueta et al., 2009; Karl et al., 2021), Saindak and Rekodiq in Pakistan (Yao et al., 2013; Lv et al., 2017), and Zhunuo in Tibet, China (Sun et al., 2021).

The large Harizha Cu-polymetallic deposit is located in the East Kunlun metallogenic belt, with estimated ore resource of 505 kt. Ore deposits in the district include those of porphyry, skarn, and medium-low temperature hydrothermal-altered rock types (Song et al., 2013; Sun et al., 2016; Yan, 2019). In recent years, the Harizha mining district has attracted much research attention. Previous studies were mainly focused on the geological-metallogenic conditions and the ages of the ore-related magmatic rocks. Tectonism at Harizha is relatively complex: NW-trending faults are the main structures, while the NE trending faults are secondary structures. Previous works have zircon U-Pb dated the ore-bearing granodiorite porphyry (234.5 ± 4.8 Ma; Song et al., 2013) and the quartz diorite (239.3 ± 2.2 Ma; Guo et al., 2016) at Harizha to be Middle Triassic (Indosinian Orogeny). However, some workers have reported older magmatic ages (diorite: 424.7 ± 4.8 Ma; granite porphyry: 242.6 ± 2.6 Ma) at Harizha, and proposed multi-stage mineralization and a diorite and/or granite porphyry ore-material source (Wang et al., 2017). In terms of metallogenesis, geochemical analysis shows that the northern Harizha mining area in Qinghai contains mainly porphyry-hydrothermal vein-skarn polymetallic deposits (Ma et al., 2016). Lithogeochemistry research and its relationship with the Cu-polymetallic mineralization is largely inadequate, and the mineralization age remains controversial. In this study, we conducted LA-ICP-MS zircon U-Pb dating and whole-rock geochemical analysis on the Harizha deposit, and discuss the ore genesis and tectonic setting.

2 Geological background

2.1 Geologic setting

The East Kunlun Orogen is a key metallogenic belt in China, and is located in the tectonically active belt of the northern Qinghai-Tibetan Plateau. The belt is located in the southern margin of the Chaidam basin and the northern margin of the Paleo-Tethys tectonic domain (Qian et al., 2000; Pan et al., 2009; Shao et al., 2017; Wu et al., 2020). The strong magmatism has led to the formation of a giant granite belt and many sizeable hydrothermal deposits (Figure 1) (Li, 2010; Du et al., 2012; Wang, 2014), including those of shallow low-temperature hydrothermal, orogenic, and hydrothermal-sedimentary types. Many metal and non-metallic minerals with development value had been discovered. It is one of the most important Mo-polymetallic metallogenic belts in Qinghai Province (Qi, 2015;

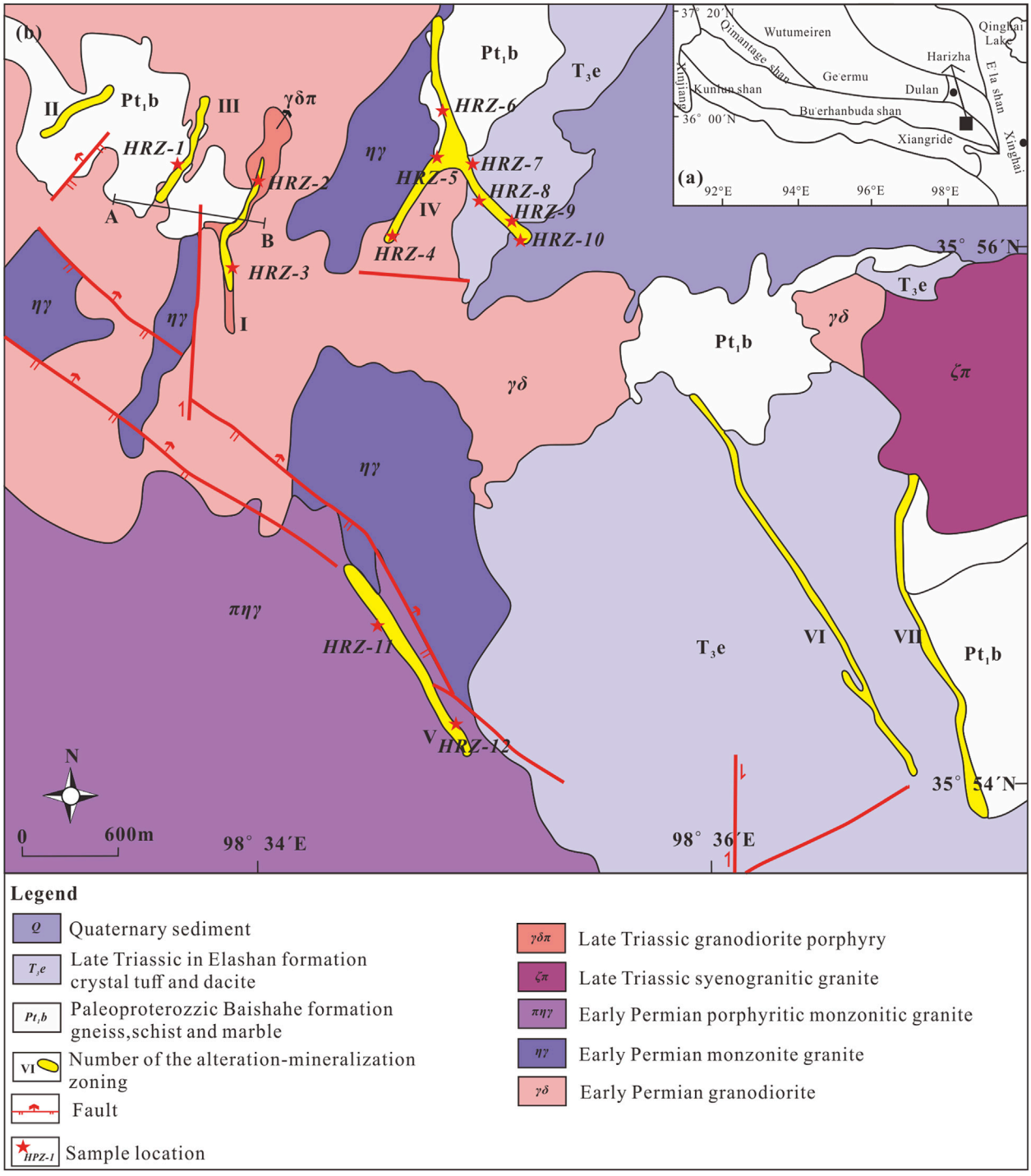

FIGURE 2
(A) Geotectonic map of Harizha; **(B)** Geological map of the Harizha deposit, showing the sampling locations (modified after Ma et al., 2016).

Han J. J. et al., 2020; Lei et al., 2020; Li Y. J. et al., 2020). Under the influence of Elashan collision-extensional orogeny, the intermediate-felsic magma in the eastern East Kunlun ore belt may have ascent along the regional NW-trending deep faults, and produce strong dissolution to surrounding strata, forming the widely-distributed intermediate-felsic plutonic and volcanic rocks. During this period, granitic magma may have formed by partial melting of crustal material under intraplate extension.

During the late Indosinian to early Yanshanian orogeny (227–205 Ma), the intermediate-felsic magma may have formed the granite-granodiorite porphyries of various sizes (Wang K. et al., 2020; Zhang et al., 2020; Zhou et al., 2020). At present, the porphyry deposits are mainly concentrated in the western part of the belt, with the Harizha deposit being a rare exception in the eastern part of the belt.

At Harizha (Dulan County, Qinghai Province), the main tectonic-magmatic activities occurred mainly in the Caledonian-Yanshanian (Yang et al., 2015; Feng et al., 2017). The deposit is 7.8 km long, 7.1 km wide, 4,200 m in elevation (max 4,767 m) (Zhong, 2018; Zhang et al., 2019). Exposed strata include mainly the Paleoproterozoic Baishahe Formation, Upper Triassic Elashan Formation, Neogene Youshashan Formation, and Quaternary sediments (Figure 2). The ore-related lithologies include mainly the granodiorite, monzogranite, and their porphyries. The wallrocks have undergone varying degrees of alteration, including mainly chlorite, epidote, sericite, and silicic.

The deposit is located between the northern Kunlun fault and central Kunlun fault, and has recorded multi-stage of tectonic-magmatic activities in the Early Paleozoic (Caledonian), Late Paleozoic (Variscan), and Triassic (Indosinian). Structures are well-developed and complex, and are dominated by compressional/transpressional faults with rare folds. The faults are NE-, NW-, and EW-trending, among which the NE- and NW-trending ones are ore-hosting (Ma et al., 2013).

Magmatic rocks are multiphase and widely distributed. Intrusive rocks include mainly gabbro, granodiorite (porphyry) and monzogranite (porphyry). The volcanic rocks include mainly the Elashan Formation dacite crystal tuff and (minor) dacite. Our study focused mainly on the ore-related granodiorite porphyry and granodiorite porphyry, whose petrographic features are described below:

Granodiorite porphyry (Figure 3A) is grayish-white (Figure 3B) and massive, and comprises phenocrysts (~40 vol %) and groundmass (~60 vol%). The phenocrysts (size: 0.1–3.5 mm) include mainly quartz, plagioclase, and biotite, and minor muscovite, hornblende, and K-feldspar. The phenocrysts are randomly distributed and euhedral-subhedral. The groundmass is composed mainly of plagioclase and quartz, with minor dark minerals. Secondary minerals include kaolinite, calcite and sericite.

The granite porphyry (Figure 3C) is grayish-white/pink (Figure 3D) and massive, and comprises phenocrysts (~25 vol %) and groundmass (~75 vol%). The phenocrysts (size: 0.2–2.5 mm) include plagioclase, K-feldspar, quartz, and biotite. The phenocrysts are randomly distributed. The groundmass is composed of quartz and feldspar laths with minor biotite. Secondary minerals include mainly sericite and kaolinite.

2.1.1 Mineralization

A total of seven mineralization belts (zone I-VII) have been identified (Figure 1). Mineralization belt I occurs in the granodiorite porphyry, and the alteration styles include mainly silicic, sericite, K-feldspar, propylitic, and kaolinite. Mineralization belt II occurs in the biotite plagioclase gneiss, and the alteration style is mainly silicic. Mineralization belt III is hosted in the granodiorite and the biotite plagioclase gneiss. Mineralization belt IV is located in the northeast tectonic fracture zone. Mineralization belt V and VI occur in the altered fracture zone and crystal tuff, respectively. Ore minerals include mainly chalcopyrite, pyrite, and malachite. Ore minerals include mainly chalcopyrite, pyrite, and malachite. (Xia, 2018; Guo et al., 2019; Li, 2019).

The copper ore samples have vein-disseminated structure (Figure 3E) and are semi-automorphic-heteromorphic granular. The ores (Figure 3F) contain mainly pyrite (25 vol%), galena (10 vol%), and chalcopyrite (1 vol%), together with non-metallic minerals (55 vol%) of plagioclase, quartz, and biotite.

The lead ore samples have also vein-disseminated structure (Figure 3G) and are semi-automorphic-heteromorphic granular. The ores (Figure 3H) have mainly galena (30 vol%), pyrite (15 vol %), sphalerite (2 vol%), arsenopyrite (8 vol%), and chalcopyrite (1 vol%), and non-metallic minerals (about 38 vol%) of plagioclase, quartz, and calcite. Lead mineralization occurs mainly in zones VI to VI.

2.1.2 Alteration

The wallrock alterations include silicic, sericite, potassic, kaolinite, chlorite and carbonate. Among which the former two are closely ore-related and widely developed. Quartz veins are relatively well-developed (Figure 4A), and often accompanied by pyritization (Figure 4B). Secondly, kaolinization, potassium and chloritization are developed (Figure 4D). Malachite (Figure 4C) and limonite supergene ores are developed on/near the surface. Therefore, the alteration zoning can be divided into: K-felsparization-sericitization-propylitization (Figure 5). The main orebodies are located in the outer part of the potassic zone and the sericite zone, similar to typical porphyry copper deposits (Lv et al., 2017).

3 Samples and methods

The sampling locations are shown in Figure 2. The samples were collected for thin-section petrography, LA-ICP-MS zircon U-Pb dating, and whole-rock geochemical analysis. The ore-related granodiorite porphyry and monzogranite porphyry were zircon U-Pb dated, whilst samples analyzed for whole-rock geochemistry include monzogranite, (altered/mineralized) granodiorite porphyry, and syenogranite porphyry.

3.1 Zircon U-Pb dating

The selected zircon was mounted with epoxy resin, and is then polished into half the thickness. LA-ICP-MS zircon U-Pb

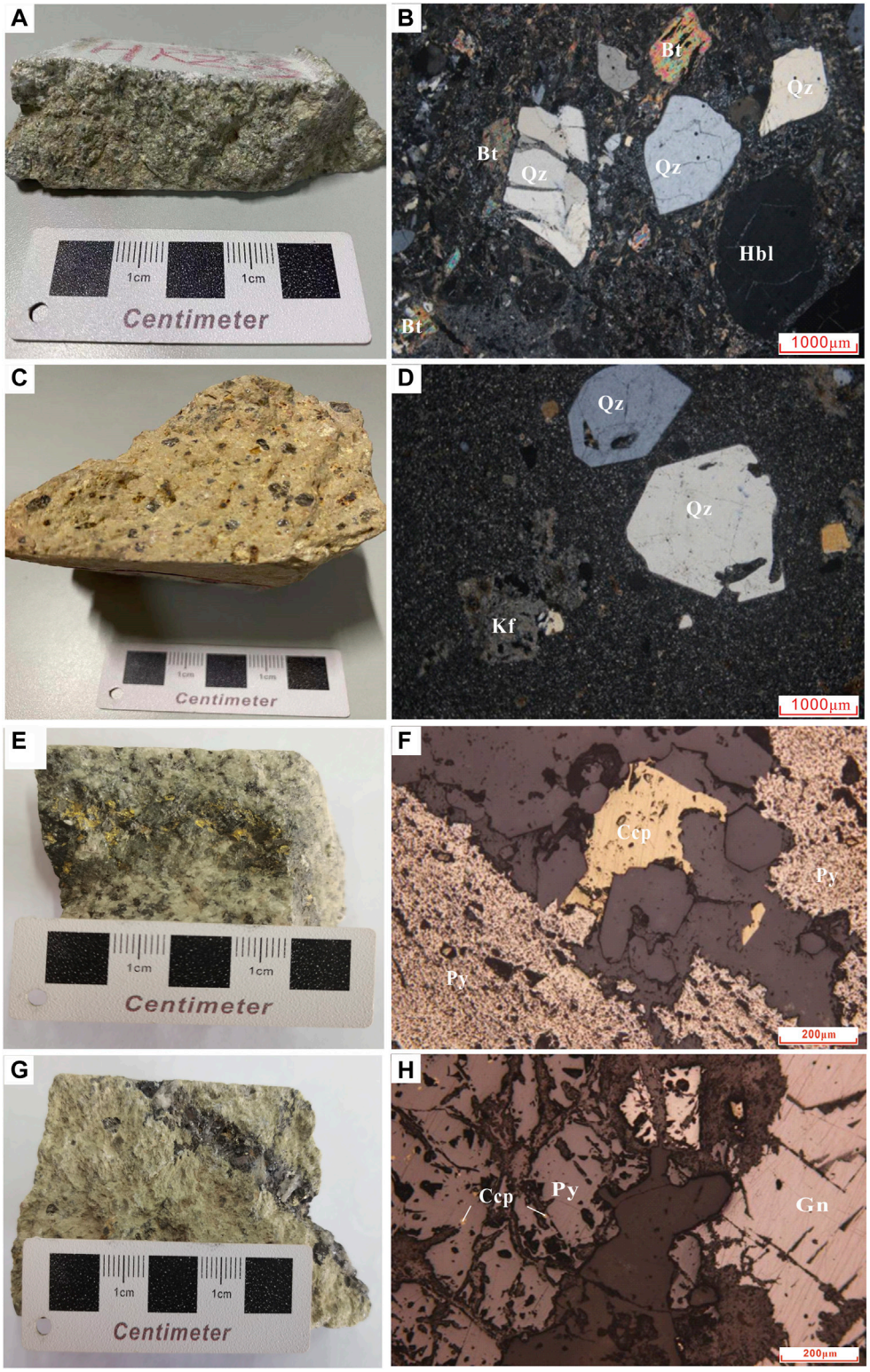

FIGURE 3
Representative photographs of rock and ore samples and corresponding micrographs of major mineral assemblages of the Harizha Cu deposit **(A)**. granodiorite porphyry; **(B)**. porphyritic texture; **(C)**. granite porphyry; **(D)**. porphyritic-matrix microcrystalline texture; **(E)**. copper ore samples; **(F)**. microscopic image of copper ore; **(G)**. lead ore samples;**(H)** microscopic image of lead ore; Pl-Plagioclase; Kfs-K-feldspar; Qz-Quartz; Bt-Biotite; Hbl-Hornblende; Py-Pyrite; Gn-Galena; Ccp-Chalcopyrite).

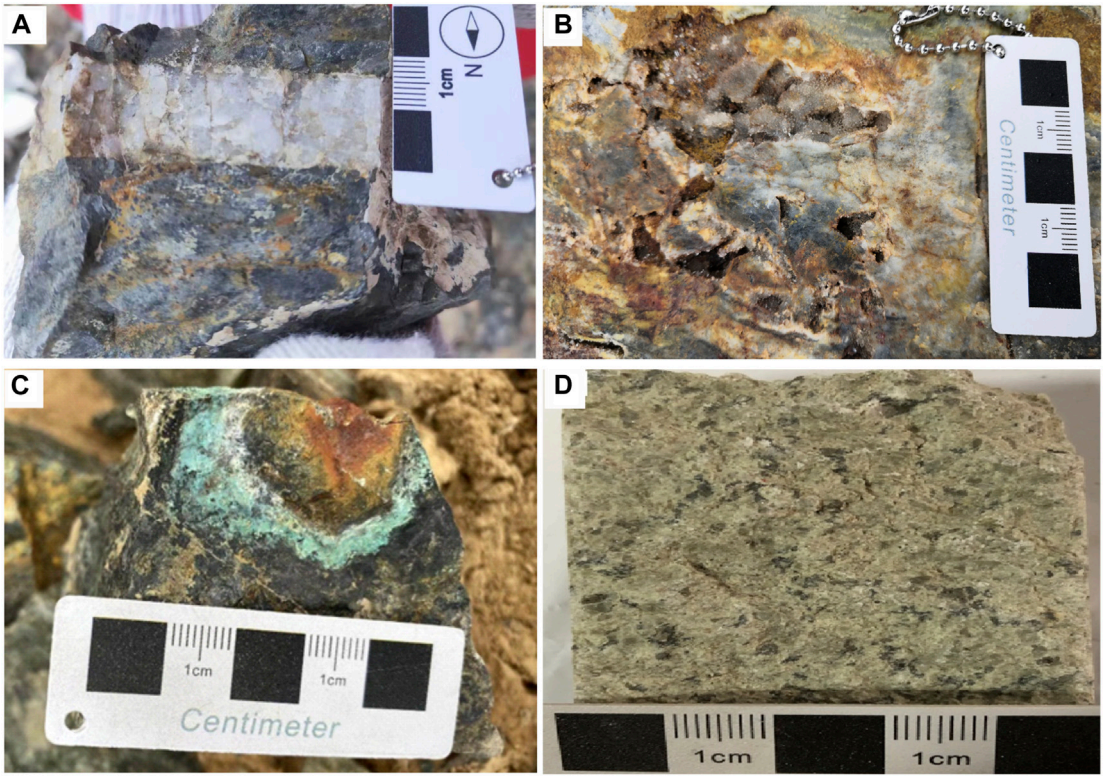

FIGURE 4
Photos showing the characteristics of ores and wallrock alteration at the Harizha deposit: **(A)**. Quartz veins; **(B)**. Pyrite associated with quartz veins; **(C)**. Malachite; **(D)**. Chloritization.

dating used an Agilent 7500 ICP-MS, a Geo Las 200 M optical system, and a Com Pex 102 ArF excimer laser. Helium was used as the carrier gas. 91500 were used as the external standards, and each standard was measured once every six samples. GJ-1 zircon standard sample was analyzed as an unknown to monitor the stability of the test process. NIST610 is used as an external standard to calculate the content of U and Th in zircon to ensure the accuracy of the test process. NIST610 and GJ-1 were measured once every 20 samples. Detailed analytical procedures are as described in Horn, Rudnick, and McDonough (2000) and Yuan et al. (2003). The data were processed using the Glitter program, and the age calculation and concordia plotting were conducted using Isoplot 3 (2006).

3.2 Zircon Hf isotope analysis

Based on zircon U-Pb dating, LA-MC-ICP-MS Hf isotope analysis was performed on the same or nearby zircon spots on the granodiorite porphyry and granite porphyry. This study was performed using a GeoLas Pro laser-ablation system coupled to a Neptune multiple-collector ICP-MS. A stationary laser ablation spot with a beam diameter of 32 μm was used for the analyses. The ablated aerosol was carried by helium and then combined with argon in a mixing chamber before being introduced to the ICP-MS plasma. A total of 10 spots were analyzed for each sample, and the raw data were processed with the Hfllow macro program.

3.3 Whole-rock geochemical analysis

Whole-rock major element contents were measured with an Axiosmax X-ray fluorescence (XRF) spectrometer. First, 500–1,000 mg samples were place in an oven for 200 min. After cooling to room temperature, the samples were weighed and the loss on ignition was calculated. Then, 600 mg of the sample was added with Li_3BO_3 and cosolvent, and the mixture was fully mixed and fused into a glass disc at high temperature. After cooling, the sample was analyzed by X-ray fluorescence spectrometer. The analysis accuracy is better than 1%. The trace element compositions were analyzed with an X Series 2 ICP-MS. HNO_3, HF, and $HClO_4$ were added to 50 mg sample to dissolve it completely, and then the solution was analyzed after cooling and dilution. The analysis accuracy is better than 5–10%. The ambient temperature of chemical analysis was 18–27 °C, with relative humidity of 25–50%.

10.3389/feart.2022.963351

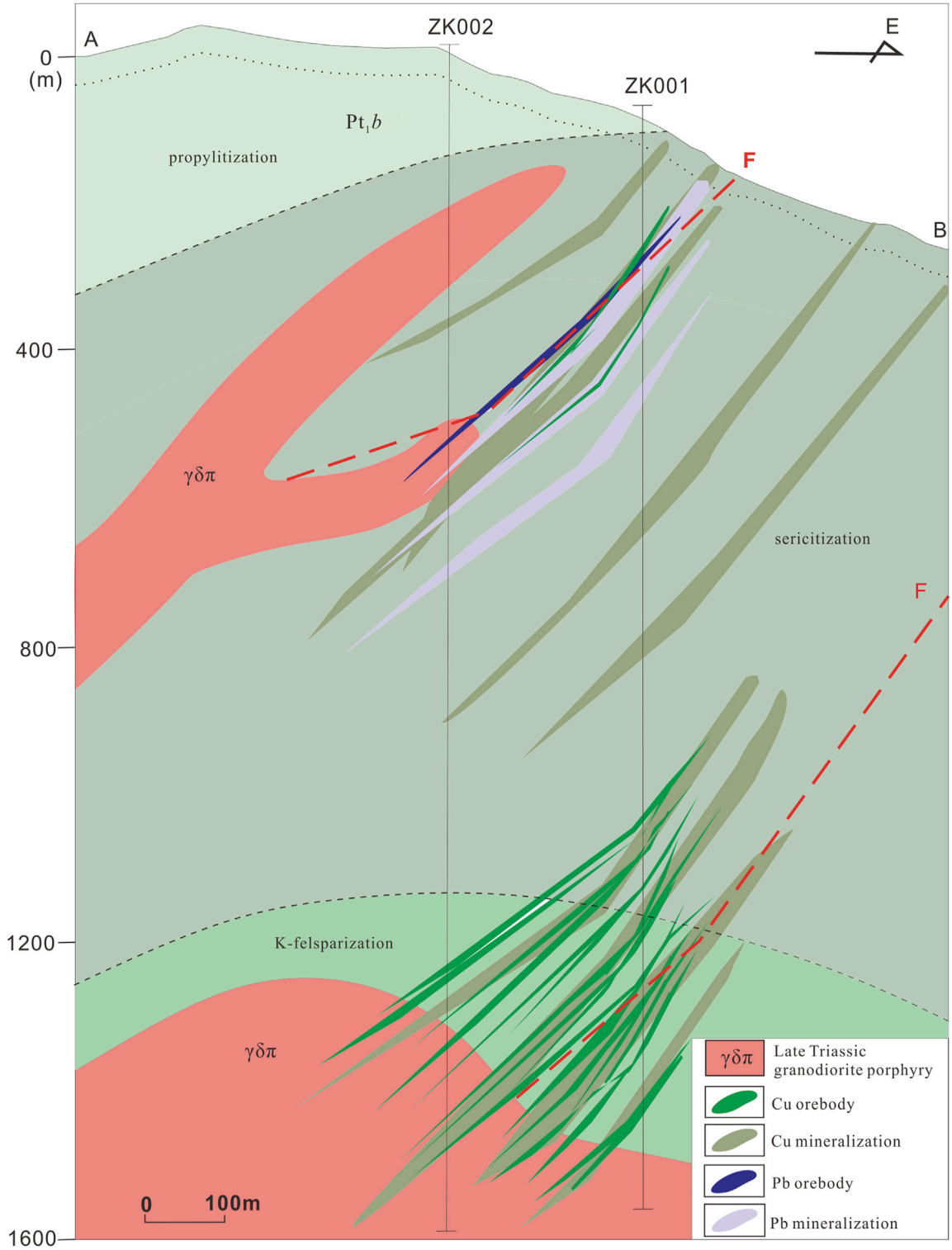

FIGURE 5
Geological profile of the Harizha mineralization zone I and orebodies.

TABLE 1 LA-MC-ICP-MS zircon U-Pb isotope dating results for the Harizha.

Sample and point number	Isotopic content/ppm			Isotope ratio						Isotopic age/Ma					
	Th	U	Th/U	$^{207}Pb/^{206}Pb$	2σ	$^{207}Pb/^{235}U$	2σ	$^{206}Pb/^{238}U$	2σ	$^{207}Pb/^{206}Pb$	2σ	$^{207}Pb/^{235}U$	2σ	$^{206}Pb/^{238}U$	2σ
HRZ-03															
1	225	414	0.5	0.0517	0.00222	0.2384	0.01029	0.0335	0.0008	270.4	95.6	217.1	8.4	212.3	5.0
2	246	647	0.4	0.0504	0.00126	0.2397	0.00631	0.0345	0.00077	213.2	56.8	218.2	5.2	218.7	4.8
3	358	664	0.5	0.0516	0.00127	0.2443	0.00635	0.0343	0.00077	268.9	55.4	222	5.2	217.6	4.8
4	326	741	0.4	0.0513	0.0014	0.2396	0.00683	0.0339	0.00076	252.6	61.7	218.1	5.6	214.9	4.8
5	504	471	1.1	0.0502	0.00144	0.2332	0.00691	0.0337	0.00076	204.1	65.2	212.8	5.7	213.6	4.7
6	428	744	0.6	0.0510	0.0014	0.2435	0.00693	0.0347	0.00078	239.3	62.0	221.3	5.7	219.6	4.9
7	320	558	0.6	0.0557	0.00141	0.2620	0.00693	0.0341	0.00076	440.9	55.0	236.3	5.6	216.2	4.8
8	117	177	0.7	0.0523	0.00235	0.2492	0.01118	0.0346	0.00083	299.7	99.3	225.9	9.1	218.9	5.2
9	430	780	0.6	0.0550	0.00209	0.2625	0.01002	0.0346	0.00081	411.7	82.1	236.7	8.1	219.4	5.0
10	211	285	0.7	0.0523	0.0025	0.2465	0.01172	0.0342	0.00083	298	105.5	223.7	9.6	216.7	5.2
11	400	478	0.8	0.0506	0.00131	0.2406	0.0065	0.0345	0.00077	221.5	58.9	218.9	5.3	218.6	4.8
12	324	525	0.6	0.0504	0.00149	0.2382	0.00724	0.0343	0.00077	211.9	67.2	216.9	5.9	217.3	4.8
13	278	657	0.4	0.0499	0.00131	0.2386	0.00651	0.0347	0.00077	188.4	60.0	217.3	5.3	219.9	4.8
14	422	886	0.5	0.0543	0.00144	0.2566	0.00706	0.0343	0.00076	382.1	58.5	231.9	5.7	217.3	4.7
15	282	774	0.4	0.0514	0.00119	0.2425	0.00591	0.0342	0.00075	259.3	52.3	220.5	4.8	216.8	4.7
16	373	850	0.4	0.0516	0.00177	0.2471	0.00857	0.0347	0.00079	268.4	76.7	224.2	7.0	219.9	4.9
17	356	618	0.6	0.0516	0.00147	0.2445	0.00715	0.0343	0.00076	268.6	64.1	222.1	5.8	217.6	4.8
18	174	621	0.3	0.0505	0.00163	0.2373	0.00775	0.0340	0.00077	219.4	72.9	216.2	6.4	215.7	4.8
19	216	353	0.6	0.0520	0.00267	0.2396	0.0122	0.0334	0.00081	283.9	113.5	218.1	10.0	211.9	5.1
20	219	522	0.4	0.0487	0.00129	0.2306	0.00633	0.0344	0.00076	131.4	61.4	210.7	5.2	217.7	4.7
21	202	562	0.4	0.0491	0.00123	0.2322	0.00606	0.0343	0.00075	151.5	57.9	212	5.0	217.3	4.7
22	228	562	0.4	0.0494	0.00135	0.2318	0.00653	0.0340	0.00075	164.3	62.9	211.6	5.4	215.7	4.7
23	222	541	0.4	0.0488	0.00144	0.2308	0.00704	0.0343	0.00077	140.1	67.9	210.8	5.8	217.2	4.8
24	174	656	0.3	0.0517	0.0013	0.2449	0.00648	0.0343	0.00077	273.6	56.5	222.4	5.3	217.5	4.8
25	610	1,417	0.4	0.0503	0.00169	0.2381	0.00816	0.0343	0.00079	208	76.1	216.9	6.7	217.6	4.9
26	160	430	0.4	0.0524	0.00147	0.2454	0.00718	0.0340	0.00077	302.1	62.8	222.9	5.9	215.4	4.8
27	210	512	0.4	0.0527	0.00141	0.2511	0.00701	0.0346	0.00078	314.9	59.5	227.4	5.7	219	4.8
28	159	243	0.7	0.0522	0.00391	0.2474	0.01829	0.0344	0.00095	292.7	162.5	224.5	14.9	217.9	5.9
29	253	816	0.3	0.0511	0.00123	0.2396	0.00613	0.0340	0.00076	243.5	54.6	218.1	5.0	215.7	4.7
30	431	858	0.5	0.0517	0.00197	0.2460	0.00951	0.0345	0.00081	270.3	85.3	223.3	7.8	218.8	5.0
31	233	562	0.4	0.0492	0.00136	0.2342	0.00675	0.0345	0.00078	155.1	63.4	213.6	5.6	218.9	4.9

(Continued on following page)

10.3389/feart.2022.963351

TABLE 1 (*Continued*) LA-MC-ICP-MS zircon U-Pb isotope dating results for the Harizha.

Sample and point number	Isotopic content/ppm			Isotope ratio						Isotopic age/Ma					
	Th	U	Th/U	$^{207}Pb/^{206}Pb$	2σ	$^{207}Pb/^{235}U$	2σ	$^{206}Pb/^{238}U$	2σ	$^{207}Pb/^{206}Pb$	2σ	$^{207}Pb/^{235}U$	2σ	$^{206}Pb/^{238}U$	2σ
32	256	552	0.5	0.0489	0.00129	0.2327	0.00646	0.0345	0.00078	144.8	60.8	212.5	5.3	218.5	4.8
33	579	593	1.0	0.0502	0.00139	0.2380	0.00686	0.0344	0.00078	204	62.9	216.7	5.6	217.8	4.8
HRZ-12															
1	131	203	0.6	0.0519	0.00215	0.2466	0.01031	0.0345	0.00083	278.7	92.1	223.8	8.4	218.6	5.1
2	353	316	1.1	0.0496	0.00152	0.2340	0.00741	0.0342	0.00079	176	69.8	213.5	6.1	216.9	4.9
3	171	236	0.7	0.0511	0.00221	0.2447	0.01064	0.0348	0.00084	242.9	96.6	222.2	8.7	220.3	5.2
4	222	520	0.4	0.0501	0.00163	0.2342	0.00785	0.0339	0.00079	197.8	74.0	213.6	6.5	215.1	4.9
5	218	407	0.5	0.0494	0.00158	0.2348	0.00773	0.0345	0.0008	164.8	73.0	214.1	6.4	218.6	5.0
6	120	211	0.6	0.0520	0.0041	0.2402	0.01864	0.0335	0.00096	284.8	170.5	218.6	15.3	212.5	6.0
7	449	804	0.6	0.0523	0.00164	0.2412	0.00782	0.0334	0.00077	300.4	69.9	219.4	6.4	211.9	4.8
8	332	616	0.5	0.0541	0.00268	0.2661	0.01316	0.0357	0.00089	375.6	107.2	239.6	10.6	225.9	5.5
9	157	385	0.4	0.0493	0.00202	0.2297	0.00951	0.0338	0.00081	164.1	93.0	209.9	7.9	214	5.0
10	127	198	0.6	0.0484	0.00268	0.2331	0.01287	0.0349	0.00088	120.3	125.7	212.7	10.6	221.1	5.5
11	234	298	0.8	0.0504	0.00168	0.2417	0.00828	0.0348	0.00081	213.1	75.5	219.8	6.8	220.4	5.0
12	178	215	0.8	0.0498	0.00169	0.2372	0.00825	0.0345	0.0008	186.3	77.1	216.1	6.8	218.8	5.0
13	123	252	0.5	0.0512	0.00198	0.2426	0.00952	0.0344	0.00081	250.2	86.7	220.5	7.8	217.7	5.1
14	200	328	0.6	0.0511	0.0017	0.2432	0.00829	0.0345	0.0008	245.9	74.6	221	6.8	218.7	5.0
15	196	317	0.6	0.0503	0.00163	0.2414	0.00804	0.0348	0.00081	210.5	73.2	219.6	6.6	220.4	5.0
16	99	179	0.6	0.0519	0.0018	0.2438	0.00866	0.0341	0.0008	280.5	77.4	221.5	7.1	216	5.0
17	155	279	0.6	0.0517	0.00176	0.2463	0.00858	0.0346	0.00081	272.5	75.9	223.6	7.0	219	5.0
18	140	267	0.5	0.0503	0.00155	0.2402	0.00766	0.0347	0.0008	207.6	69.8	218.6	6.3	219.6	5.0
19	158	283	0.6	0.0525	0.0025	0.2429	0.01158	0.0336	0.00083	307.2	104.9	220.8	9.5	212.7	5.2
20	94	181	0.5	0.0528	0.00237	0.2492	0.01126	0.0342	0.00083	318.9	99.0	225.9	9.2	217.1	5.2
21	239	271	0.9	0.0506	0.00152	0.2422	0.00756	0.0347	0.0008	222.2	67.9	220.2	6.2	220	5.0
22	636	573	1.1	0.0522	0.00141	0.2494	0.00711	0.0347	0.00079	293.6	60.6	226.1	5.8	219.7	4.9
23	160	192	0.8	0.0480	0.0019	0.2245	0.00895	0.0339	0.00079	99	92.2	205.7	7.4	214.9	4.9
24	348	665	0.5	0.0501	0.00124	0.2344	0.00608	0.0339	0.00075	201.2	56.3	213.8	5.0	214.9	4.7
25	277	345	0.8	0.0506	0.00157	0.2376	0.00754	0.0341	0.00077	221.5	70.1	216.5	6.2	216	4.8
26	141	275	0.5	0.0517	0.00172	0.2412	0.00819	0.0339	0.00077	270	74.7	219.4	6.7	214.7	4.8
27	76	141	0.5	0.0481	0.00294	0.2246	0.01358	0.0339	0.00086	104.5	138.4	205.7	11.3	214.6	5.4
28	303	499	0.6	0.0505	0.00141	0.2352	0.00682	0.0338	0.00076	215.9	63.5	214.5	5.6	214.3	4.7

(Continued on following page)

10.3389/feart.2022.963351

10.3389/feart.2022.963351

TABLE 1 (*Continued*) LA-MC-ICP-MS zircon U-Pb isotope dating results for the Harizha.

Sample and point number	Isotopic content/ppm			Isotope ratio						Isotopic age/Ma					
	Th	U	Th/U	$^{207}Pb/^{206}Pb$	2σ	$^{207}Pb/^{235}U$	2σ	$^{206}Pb/^{238}U$	2σ	$^{207}Pb/^{206}Pb$	2σ	$^{207}Pb/^{235}U$	2σ	$^{206}Pb/^{238}U$	2σ
29	215	354	0.6	0.0503	0.0015	0.2377	0.0073	0.0343	0.00077	207.9	67.8	216.5	6.0	217.3	4.8
30	190	331	0.6	0.0485	0.00153	0.2301	0.00743	0.0344	0.00078	123.3	72.6	210.3	6.1	218.1	4.9
31	93	178	0.5	0.0494	0.00181	0.2291	0.0085	0.0336	0.00077	168.1	83.3	209.4	7.0	213.1	4.8
32	175	240	0.7	0.0502	0.00164	0.2362	0.00789	0.0341	0.00078	202.4	74.1	215.3	6.5	216.4	4.9
33	241	390	0.6	0.0511	0.00154	0.2403	0.00746	0.0341	0.00077	247	68.1	218.6	6.1	215.9	4.8

4 Results

4.1 LA-ICP-MS zircon U-Pb dating

Zircon U-Pb dating was carried out on two samples from Harizha. The data are presented in Table 1, whilst representative zircon cathodoluminescence (CL) images and analytical spots are shown in Figure 6. The analyzed zircons are euhedral long columnar and (minor) short columnar, with aspect ratios of 1:1 to 3:1. Oscillatory zoning is well developed, and the high Th/U values (0.3–1.1) resemble typical magmatic zircons. Therefore, the U-Pb age can reflect the rock crystallization age (Hoskin and Schaltegger 2003; Wang et al., 2014; Yang et al., 2020).

A total of 33 spots were measured for the granodiorite porphyry (HRZ-3) (Table 1). The zircons have Th = 116.99–610.14 ppm, U = 177.49–1,416.97 ppm, Th/U = 0.20–1.27, and $^{206}Pb/^{238}U$ = 211.9–219.9 Ma. All the 33 zircon spots are concordant and plot on/near the concordia (Figures 7A, B). The weighted average age (217.3 ± 1.8 Ma; MSWD = 0.17) likely represents the crystallization age of the granodiorite porphyry.

A total of 33 spots were measured for the granite porphyry (HRZ-12) (Table 1). The zircons have Th = 75.54–635.59 ppm, U = 140.56–804.24 ppm, Th/U = 0.52–0.79, and $^{206}Pb/^{238}U$ = 211.9–225.9 Ma. All the 33 zircon spots are concordant and plot on/near the concordia (Figure 7C, D). The weighted average age (217.0 ± 1.7 Ma; MSWD = 0.35) likely represents the crystallization age of the granite porphyry.

4.2 Zircon Hf isotopes

The study performed 40 Hf isotope spot analyses on the granodiorite porphyry and granite porphyry (20 spots each) (Table 2). Twenty analyses on the granodiorite porphyry yielded $^{176}Lu/^{177}Hf$ = 0.000611–0.001957, $^{176}Hf/^{177}Hf$ = 0.282,417–0.282,510, and $\varepsilon_{Hf}(t)$ = -7.98 to -4.58, $f_{Lu/Hf}$ = -0.98 to -0.94. Calculated zircon two-stage Hf model age (T_{DM2}) = 1.5 to 1.8 Ga. Twenty analyses on the granite porphyry yielded $^{176}Lu/^{177}Hf$ = 0.000585–0.001118, $^{176}Hf/^{177}Hf$ = 0.282,442–0.282,509, and $\varepsilon_{Hf}(t)$ = -6.89 to -4.65, $f_{Lu/Hf}$ = -0.98 to -0.97. Calculated zircon two-stage Hf model age (T_{DM2}) = 1.5 to 1.7 Ga.

4.3 Whole-rock geochemical compositions

The rock samples have SiO_2 = 68.44–78.13 wt% (avg. 73.06 wt%), K_2O = 0.75–5.46 wt% (avg. 4.22 wt%), total alkali (K_2O+Na_2O) = 4.03–8.33 wt% (avg. 7.09 wt%), Al_2O_3 = 12.22–15.17 wt% (avg. 13.86 wt%), CaO = 0.44–3.65 wt% (avg. 1.50 wt%), and A/CNK = 1.02–1.68 (avg. 1.18) (Table 3).

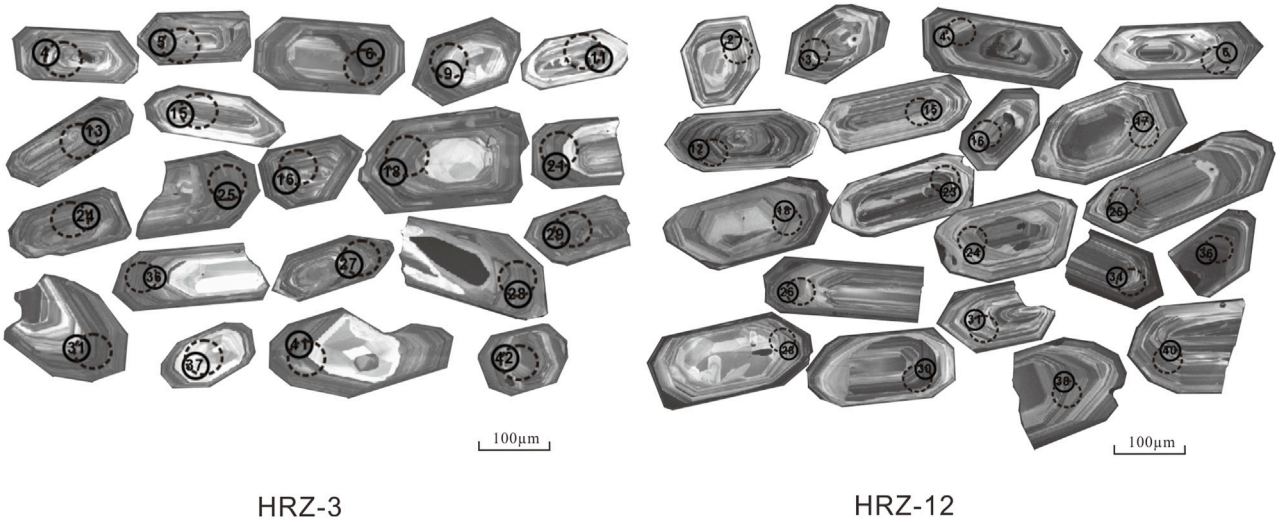

FIGURE 6
Representative zircon CL images of the Harizha granitoids. Solid-line and dotted-line circles denote the locations of U–Pb and Hf isotopic analysis spots, respectively.

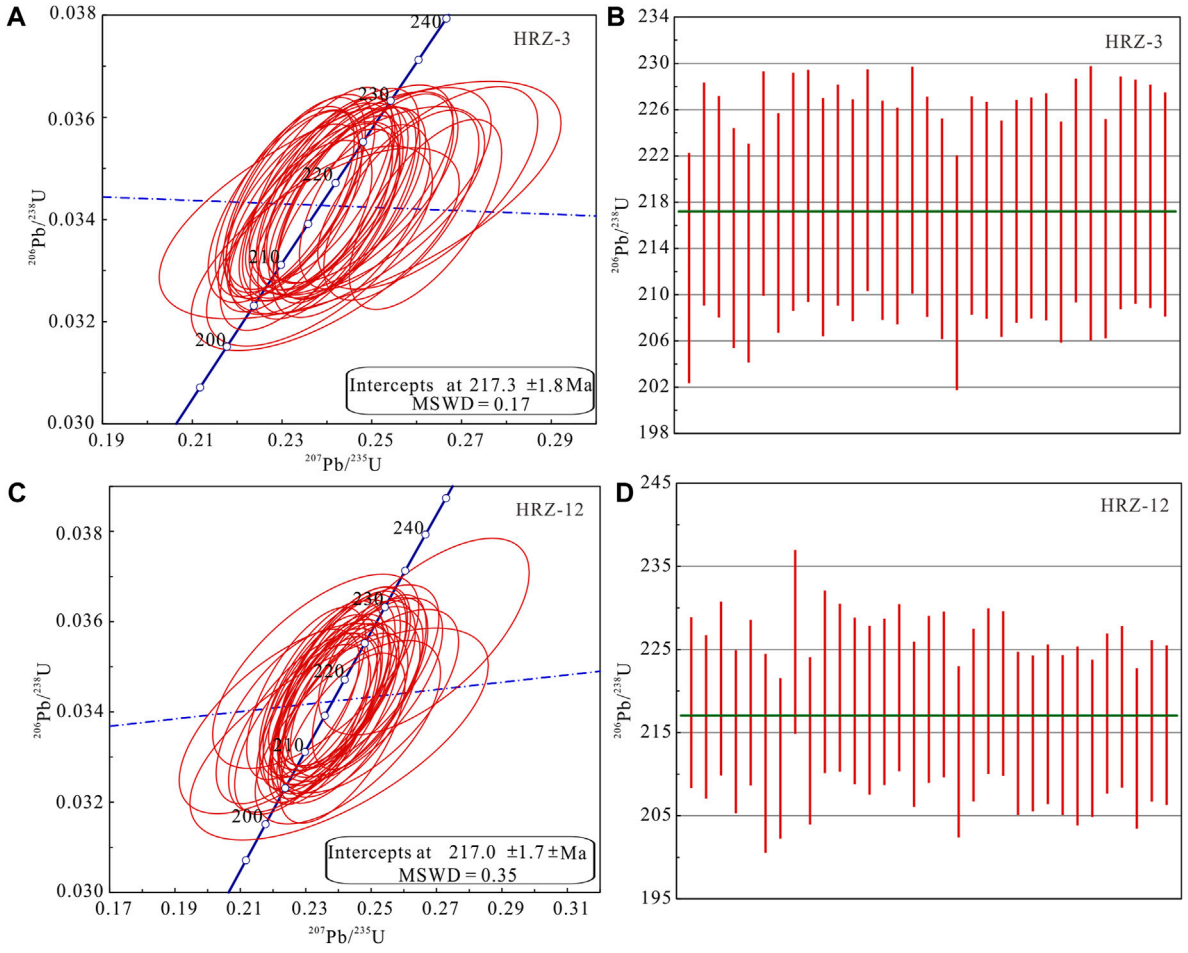

FIGURE 7
Zircon U–Pb concordia age and weighted mean age diagrams of the Harizha granitoids. **(A–D)** MSWD, mean square weighted deviation.

10.3389/feart.2022.963351

TABLE 2 Results of LA-ICP-MS Hf isotopes of zircon from the Harizha.

Point number	t (Ma)	$^{176}Yb/^{177}Hf$	$^{176}Lu/^{177}Hf$	$^{176}Hf/^{177}Hf$	$\varepsilon_{Hf}(0)$	±1σ	$\varepsilon_{Hf}(t)$	±1σ	$T_{DM1}(Hf)$ (Ma)	$T_{DM2}(Hf)$ (Ma)	$f_{Lu/Hf}$
HRZ-03											
4	219	0.023409	0.000823	0.282,475	-10.44	0.74	-5.83	0.74	1,095	1,620	-0.98
5	218	0.029516	0.000948	0.282,437	-11.79	0.58	-7.21	0.58	1,152	1706	-0.97
6	215	0.025840	0.000823	0.282,440	-11.67	0.59	-7.14	0.59	1,143	1,699	-0.98
9	220	0.027370	0.000989	0.282,510	-9.19	0.51	-4.58	0.51	1,050	1,541	-0.97
11	219	0.039069	0.001378	0.282,430	-12.01	0.63	-7.48	0.63	1,174	1724	-0.96
13	219	0.030174	0.001048	0.282,495	-9.72	0.71	-5.14	0.71	1,073	1,576	-0.97
15	217	0.034530	0.001229	0.282,470	-10.61	0.86	-6.10	0.86	1,114	1,635	-0.96
16	219	0.059911	0.001957	0.282,419	-12.43	0.73	-7.98	0.73	1,209	1755	-0.94
18	217	0.018640	0.000611	0.282,417	-12.49	0.62	-7.89	0.62	1,169	1748	-0.98
21	217	0.021716	0.000736	0.282,425	-12.20	0.60	-7.61	0.60	1,162	1731	-0.98
24	218	0.031473	0.001046	0.282,453	-11.22	0.53	-6.66	0.53	1,132	1,671	-0.97
25	216	0.021050	0.000746	0.282,445	-11.50	0.56	-6.94	0.56	1,134	1,687	-0.98
27	218	0.026999	0.000921	0.282,473	-10.50	0.53	-5.93	0.53	1,100	1,625	-0.97
28	217	0.020878	0.000700	0.282,439	-11.72	0.56	-7.13	0.56	1,142	1700	-0.98
29	216	0.024017	0.000850	0.282,500	-9.56	0.61	-5.01	0.61	1,061	1,566	-0.97
31	217	0.030312	0.001023	0.282,458	-11.03	0.65	-6.49	0.65	1,124	1,660	-0.97
36	219	0.021892	0.000754	0.282,438	-11.75	0.51	-7.13	0.51	1,145	1702	-0.98
37	218	0.029066	0.001031	0.282,479	-10.29	0.79	-5.73	0.79	1,095	1,613	-0.97
41	219	0.023010	0.000823	0.282,461	-10.92	0.56	-6.31	0.56	1,114	1,650	-0.98
42	218	0.031473	0.001046	0.282,453	-11.22	0.53	-6.66	0.53	1,132	1,671	-0.97
HRZ-12											
2	219	0.026083	0.000964	0.282,493	-9.80	0.66	-5.21	0.66	1,074	1,580	-0.97
3	217	0.023014	0.000823	0.282,487	-10.00	0.72	-5.43	0.72	1,078	1,593	-0.98
4	220	0.022979	0.000763	0.282,492	-9.83	0.62	-5.19	0.62	1,069	1,580	-0.98
6	219	0.022265	0.000813	0.282,472	-10.56	0.68	-5.94	0.68	1,099	1,627	-0.98
12	226	0.025410	0.000972	0.282,442	-11.61	0.86	-6.87	0.86	1,146	1,691	-0.97
15	221	0.022072	0.000810	0.282,493	-9.80	0.65	-5.14	0.65	1,069	1,578	-0.98
16	220	0.029311	0.000998	0.282,490	-9.90	0.67	-5.29	0.67	1,079	1,586	-0.97
17	219	0.020417	0.000723	0.282,465	-10.78	0.62	-6.15	0.62	1,105	1,640	-0.98
18	218	0.017553	0.000604	0.282,481	-10.22	0.59	-5.60	0.59	1,080	1,604	-0.98
23	220	0.025253	0.000892	0.282,462	-10.90	0.67	-6.28	0.67	1,115	1,649	-0.97
24	216	0.018425	0.000617	0.282,469	-10.64	0.60	-6.07	0.60	1,097	1,632	-0.98
25	219	0.016809	0.000585	0.282,507	-9.30	0.66	-4.65	0.66	1,043	1,545	-0.98
26	220	0.019302	0.000681	0.282,498	-9.60	0.54	-4.95	0.54	1,058	1,565	-0.98
28	217	0.027198	0.000931	0.282,479	-10.27	0.62	-5.72	0.62	1,091	1,611	-0.97
30	220	0.033061	0.001118	0.282,448	-11.38	0.63	-6.78	0.63	1,141	1,681	-0.97
31	215	0.023751	0.000868	0.282,454	-11.17	0.59	-6.65	0.59	1,125	1,668	-0.97
34	215	0.029260	0.000972	0.282,448	-11.40	0.53	-6.89	0.53	1,137	1,684	-0.97
36	214	0.024548	0.000843	0.282,509	-9.24	0.63	-4.74	0.63	1,048	1,547	-0.97
38	218	0.017713	0.000625	0.282,459	-11.00	0.61	-6.38	0.61	1,111	1,653	-0.98
40	216	0.022412	0.000781	0.282,459	-11.01	0.66	-6.46	0.66	1,116	1,657	-0.98

In the total alkali-silica (TAS) classification diagram (Figure 8A), the rock samples plot in the subalkaline granite field. In the A/NK-A/CNK (Figure 8B) and SiO_2-K_2O (Figure 8C) diagrams, the rocks are classified as peraluminous and high-K calc-alkaline. In the (Na_2O+K_2O-CaO)/SiO_2 diagram (Figure 8D), the data points fall into the calc-alkaline field.

The rocks have total rare earth element (REE) contents of 46.13–211.16 ppm (avg. 132.05 ppm), and negative Eu anomalies

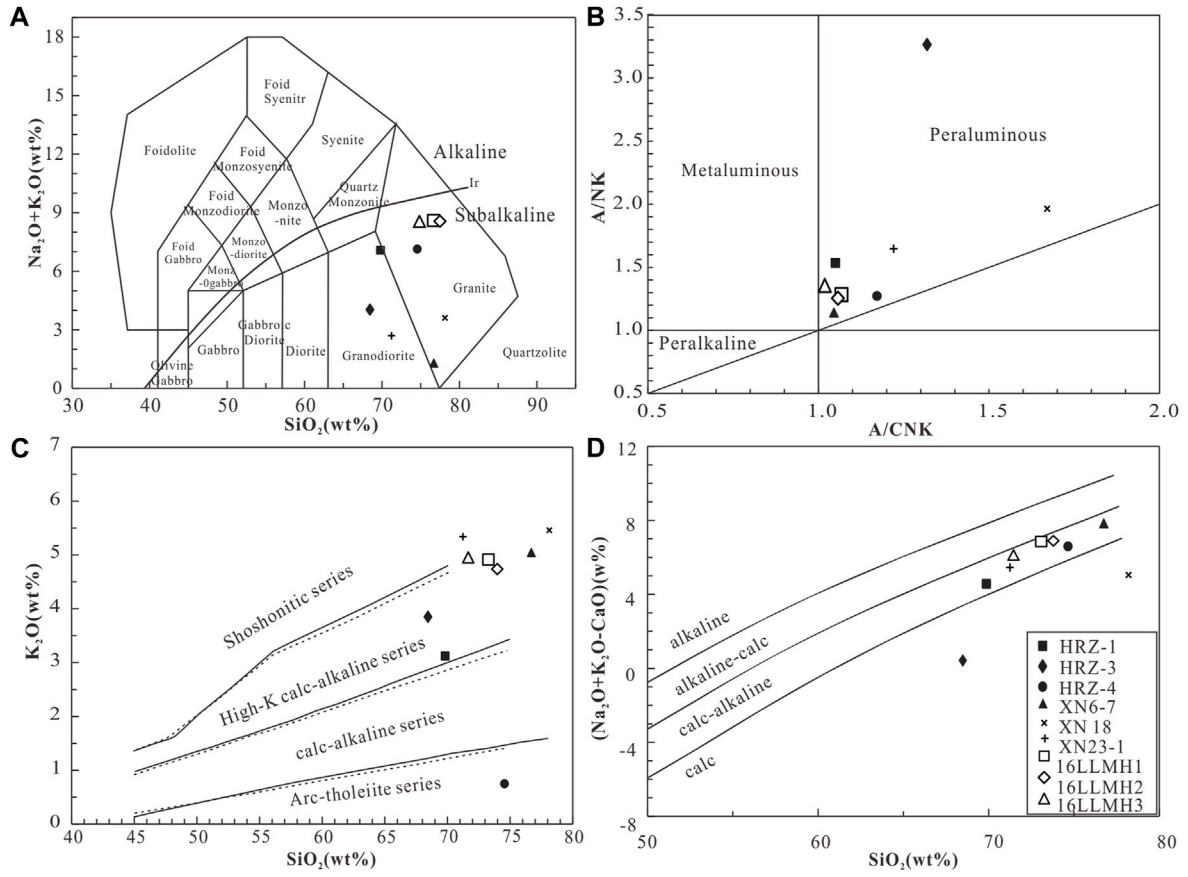

FIGURE 8
Geochemical classification diagrams for the Harizha granitoids: **(A)** TAS (after Middlemost and Sun 1985); **(B)** $Al_2O_3/(Na_2O+K_2O)$ versus $Al_2O_3/(CaO+Na_2O+K_2O)$ (Maniar and Piccoli, 1989); **(C)** K_2O versus SiO_2 (after Middlemost 1985); **(D)** (Na_2O+K_2O-CaO) versus SiO_2 (Frost et al., 2001).

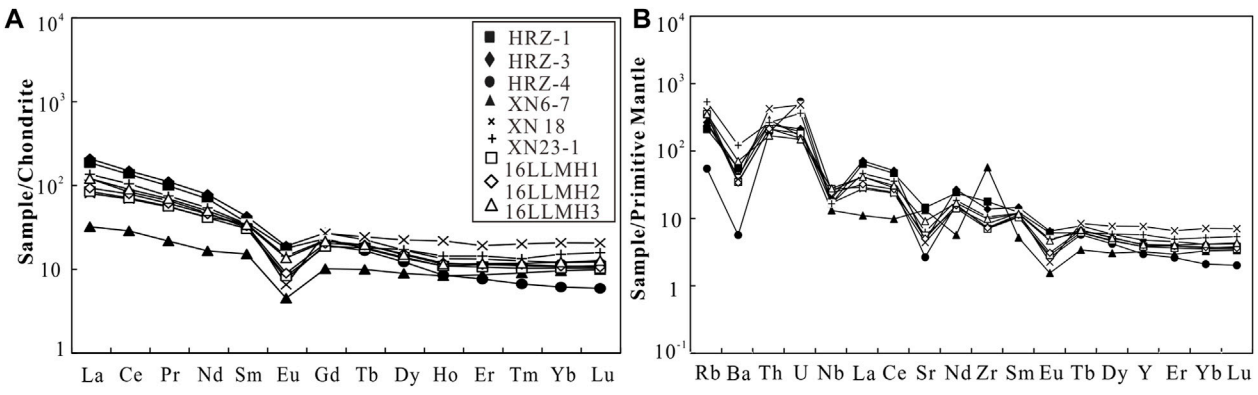

FIGURE 9
(A) Chondrite-normalized REE patterns; **(B)** Primitive mantle-normalized trace element patterns. Chondrite and primitive-mantle normalizing values are from Sun and McDonough (1989) and Rudnick and Gao (2004), respectively.

(δEu = 0.21–0.60, avg. 0.41). In the chondrite-normalized REE plot (Figure 9A), the rocks show right-inclining patterns (LREE/HREE enrichment), with LREE/HREE = 4.30–12.82, $(La/Yb)_N$ = 3.34–19.67, indicating significant fractionation (Han Z. H. et al., 2020). The rocks have slightly negative Ce anomalies (δCe = 0.89–1.07, avg. 0.98), indicating that the oxidized conditions were relatively stable during the magmatic evolution (Wang P. X. et al., 2020). In the primitive mantle-normalized multi-element spider diagram (Figure 9B), the element distribution curves of the different rock samples are similar, and are featured by enrichments in large ion lithophile elements (LILE; e.g., Rb, K), other incompatible elements (e.g., Th and U), and depletions in high field strength elements (HFSE; e.g., Nb, Th) (Table 3).

5 Discussion

5.1 Petrogenesis and magma source

-From the diagram of Zr+Nb+Ce+Y–(K_2O+Na_2O)/CaO (Figure 10A), it can be seen that most of the samples fall into the I-,S- and M-type regions of the undifferentiation granite. In the diagram of SiO_2–Zr (Figure 10B), most of the samples fall into the S-type region. In general, A/CNK = 1.1 is the threshold for distinguishing I- from S-type granite (Sylvester, 1998). The aluminum saturation index of Harizha samples is between 1.02 and 1.68 (avg. 1.18). Therefore, we speculated that the Harizha samples have the characteristics of I- to S-type transitional granite.

When discussing the magma source region, previous studies suggested that Rb/Sr > 0.5 and Nd/Th ≈ 3 indicate likely crustal material remelting during orogenic process (Gibbs, 1986; McDonough and Sun 1995; Xiao et al., 2002), similar to our samples (Rb/Sr = 0.44–2.69 (avg. 1.53); Nd/Th = 0.31–1.72 (avg. 1.15)), which indicates a crustal source for the Harizha granitoids. Meanwhile, the rocks have low Sr (56.20–306.50 ppm) but high Y (13.50–34.70 ppm) and Yb (1.04–3.51 ppm), consistent with the content of mafic rocks in the crust. The high SiO_2 and K_2O but low MgO contents, and the LREE/HREE enrichment again support a crustal magma source (Gao and Sun, 2021).

The zircon Lu-Hf isotope system has high closure temperature, and can reflect the Hf isotopes during petrogenesis (Wu et al., 2007). In this study, the $^{176}Lu/^{177}Hf$ ratios of the two samples were <0.002, and the variation range is very small. It shows that Hf isotopes are rarely accumulated after zircon formation, which can represent Hf isotopic composition of magmatic system during zircon formation (Zhang et al., 2020). The $f_{Lu/Hf}$ ratios are significantly lower than the average continental crust (-0.55) (Griffin et al., 2000). Thus, its two Hf model ages (T_{DM2}) can better reflect the average crustal retention age of the source material (Huang et al., 2016). In the Age-ε_{Hf} (t) diagram (Figure 11), the granodiorite porphyry and granite porphyry samples from Harizha fall below the meteorite evolution line. The ε_{Hf} (t) value is mainly distributed between -8 and -4, and the corresponding T_{DM2} is mainly concentrated between 1.5 and 1.8 Ga. In this study, the ε_{Hf} (t) values of granodiorite porphyry and granite porphyry are negative, indicating that the ancient crustal material was remelted.

5.2 Tectonic setting

Previous studies have shown that tectonic evolution of the East Kunlun Orogen mainly involved four stages: 1) ocean

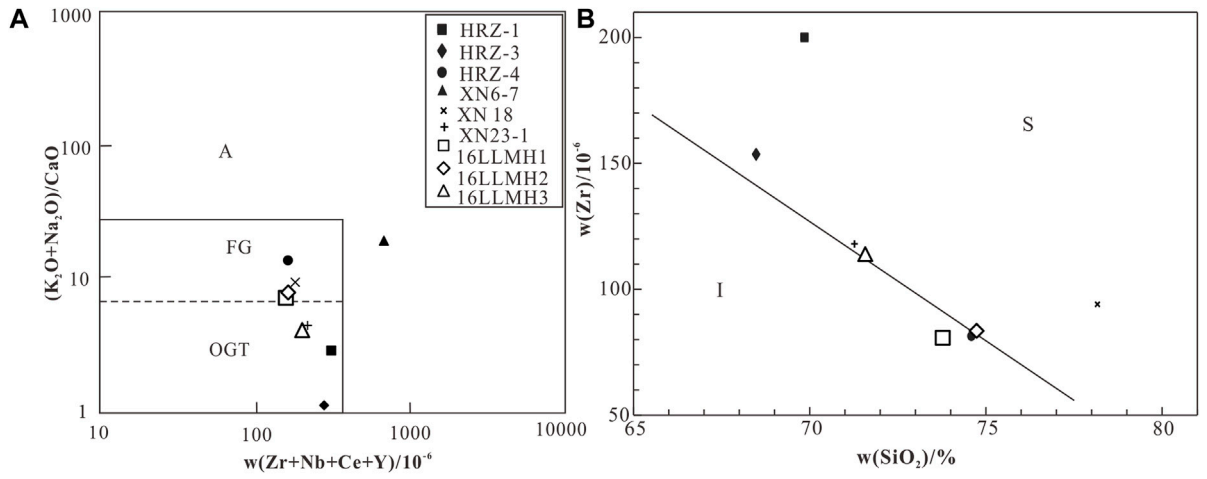

FIGURE 10
(Zr+Nb+Ce+Y) versus (K_2O+Na_2O)/CaO diagrams of Harizha (A—A-type granite; FG—Fractionated I, S, M-type granite; OGT—Non-fractionated I, S, M-type granite; I—I-type granite). **(A,B)** S-S-type granite.

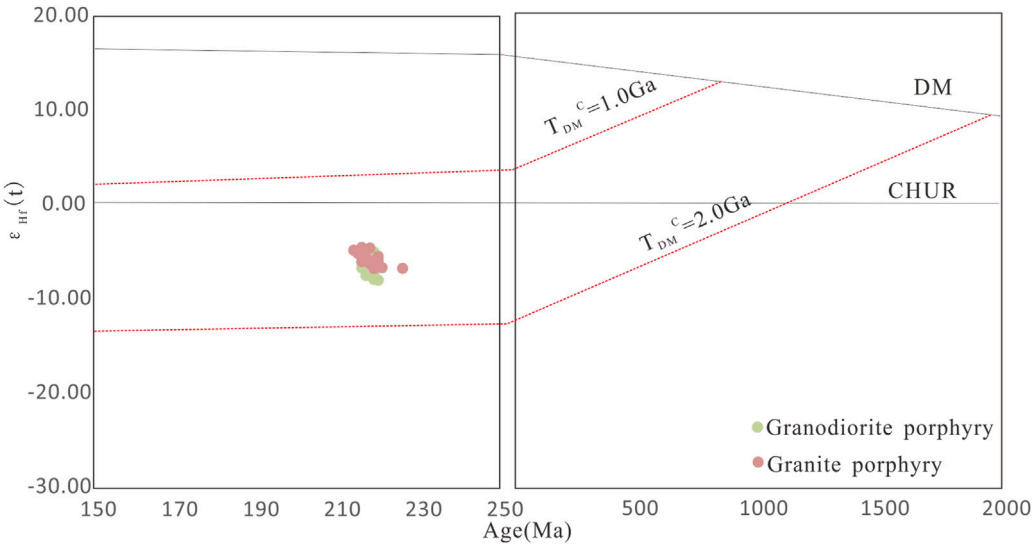

FIGURE 11
U–Pb age versus $\varepsilon_{Hf}(t)$ diagram of Lu-Hf isotopic evolution of zircon from the Harizha (Belousova et al., 2010)

basin opening and expansion (Neoarchean–Proterozoic), 2) ocean basin subduction (Early Paleozoic), 3) continent-continent collision (Late Paleozoic-Early Mesozoic), and 4) post-collisional extension (Cenozoic-Mesozoic) (Liu et al., 2013; Zhang et al., 2016). The Late Paleozoic-Early Mesozoic was the Paleo-Tethys orogenic period and was the main granite emplacement period in the East Kunlun (Xia et al., 2014; Feng et al., 2017; Xu et al., 2021). Some workers proposed that the Late Carboniferous-Late Permian (309–260 Ma) was the ocean-ridge formation and expansion stage. The Late Permian-Middle Triassic (260–230 Ma) was the ocean subduction stage. The Middle Triassic-Early Jurassic (230–190 Ma) was the intraplate orogenic stage (Guo and Deng, 1998; Li X. R. et al., 2020; Li et al., 2021). It is widely accepted that the Paleotethys have begun subduction in the East Kunlun in the Late Permian, and have changed from a subduction to a collision setting in the Middle Triassic (Guo et al., 2016; Wang K. et al., 2020; Xu et al., 2020). During the tectonic evolution, regional mantle-derived magma underplating, accompanied by partial melting of crustal rocks, may have formed voluminous calc-alkaline magmas

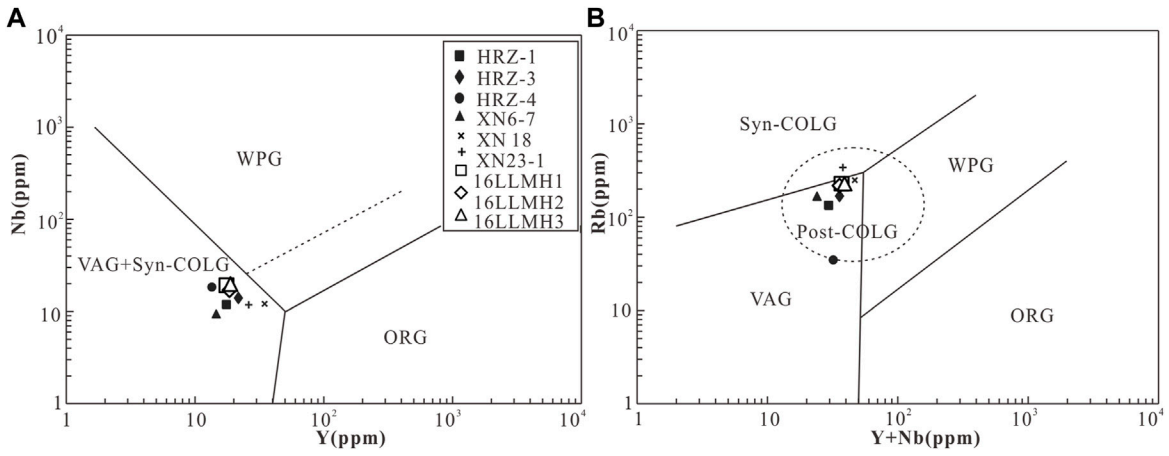

FIGURE 12
Tectonic discrimination diagrams for the Harizha granitoids: **(A)** Nb versus Y (Pearce, Harris, and Tindle, 1984); **(B)** Rb versus (Y + Nb) (Pearce, Harris, and Tindle, 1984). Abbreviations: Syn-COLG, syn-collisional granites; Post-COLG, post-collisional granites; WPG, within-plate granites. VAG, volcanic arc granites; ORG, ocean ridge granites.

TABLE 3 Major and trace element data for the Harizha.

Sample No.	HRZ-1	HRZ-3	HRZ-4	XN6-7	XN18	XN23-1	16LLMH1	16LLMH2	16LLMH3
	Monzogranite	Granodiorite porphyry	Granodiorite	Granite porphyry	Syenogranite porphyry	Mineralized Granite porphyry	Granodiorite	Granodiorite	Granodiorite
SiO_2	69.81	68.44	74.55	76.69	78.13	71.23	73.28	74.18	71.21
Al_2O_3	15.17	14.70	14.39	12.22	12.26	14.25	13.77	13.48	14.46
TiO_2	0.40	0.39	0.18	0.08	0.11	0.28	0.16	0.14	0.29
Fe_2O_3	0.41	0.40	0.22	1.25	2.54	3.06	0.53	0.33	0.44
FeO	1.95	1.50	0.79	0.82	0.37	1.49	1.03	0.92	1.44
CaO	2.49	3.65	0.53	0.44	0.61	1.62	1.13	1.03	1.97
MgO	0.96	0.97	1.04	0.16	0.31	0.86	0.53	0.39	0.62
K_2O	3.12	3.85	0.75	5.04	5.46	5.34	4.88	4.65	4.93
Na_2O	3.96	0.18	6.39	3.29	0.17	1.76	3.33	3.51	3.20
MnO	0.07	0.04	0.01	0.02	0.01	0.06	0.03	0.03	0.04
P_2O_5	0.12	0.10	0.10	0.01	0.02	0.06	0.07	0.07	0.19
LOI	1.21	5.52	0.95	-	-	-	1.21	1.23	1.22
$K_2O+ Na_2O$	7.08	4.03	7.14	8.33	5.63	7.10	8.21	8.16	8.13
Na_2O/K_2O	1.27	0.05	8.47	0.65	0.03	0.33	0.68	0.75	0.65
A/KNC	1.05	1.32	1.17	1.05	1.68	1.22	1.07	1.06	1.02
La	44.30	49.20	28.60	7.60	19.00	32.00	20.00	22.10	28.50
Ce	83.00	91.20	50.90	17.50	42.10	63.70	43.30	48.20	54.90
Pr	9.39	10.50	6.24	2.05	5.26	7.10	5.34	5.79	6.57
Nd	32.30	36.40	21.80	7.70	19.60	25.20	19.20	21.30	23.10
Sm	5.50	6.50	4.75	2.32	5.35	5.31	4.64	5.04	5.18
Eu	1.03	1.09	0.44	0.26	0.38	0.83	0.48	0.52	0.79
Gd	4.74	5.55	3.99	2.08	5.50	4.56	3.83	4.16	4.41
Tb	0.66	0.84	0.62	0.37	0.91	0.67	0.67	0.72	0.73
Dy	3.42	4.30	3.10	2.26	5.65	4.33	3.51	3.86	3.78
Ho	0.62	0.75	0.48	0.47	1.23	0.81	0.62	0.67	0.65
Er	1.88	2.18	1.26	1.41	3.16	2.38	1.75	1.87	1.93
Tm	0.28	0.32	0.17	0.23	0.51	0.34	0.26	0.29	0.30
Yb	1.81	2.04	1.04	1.63	3.51	2.56	1.75	1.85	2.06
Lu	0.28	0.31	0.15	0.25	0.52	0.40	0.26	0.27	0.32
Y	17.50	21.70	13.50	14.60	34.70	26.10	17.40	18.40	18.70
Rb	134.17	168.84	34.85	167.50	250.00	342.00	225.00	215.00	225.00

(Continued on following page)

10.3389/feart.2022.963351

TABLE 3 (*Continued*) Major and trace element data for the Harizha.

Sample No.	HRZ-1	HRZ-3	HRZ-4	XN6-7	XN18	XN23-1	16LLMH1	16LLMH2	16LLMH3
	Monzogranite	Granodiorite porphyry	Granodiorite	Granite porphyry	Syenogranite porphyry	Mineralized Granite porphyry	Granodiorite	Granodiorite	Granodiorite
Ba	391.45	294.08	39.79	389.00	269.00	852.00	245.00	238.00	499.00
Th	21.46	21.12	16.17	24.60	36.20	22.50	18.00	18.30	14.40
U	4.09	4.46	11.33	3.52	10.20	7.66	3.81	3.26	3.13
Nb	11.89	14.01	18.43	9.40	12.10	11.80	19.50	17.20	20.00
Sr	306.50	98.92	56.15	282.00	93.00	132.00	118.00	106.00	193.00
Zr	199.78	153.68	81.50	640.00	94.00	118.00	78.80	81.40	110.00
∑REE	189.26	211.16	123.57	46.13	112.68	150.19	105.61	116.64	133.22
LREE/HREE	12.82	11.96	10.43	4.30	4.37	8.36	7.35	7.52	8.39
(La/Yb)N	17.54	17.27	19.67	3.34	3.88	8.97	8.20	8.57	9.92
δEu	0.60	0.54	0.30	0.35	0.21	0.50	0.34	0.34	0.49
δCe	0.95	0.94	0.89	1.07	1.02	0.99	1.01	1.02	0.95
Rb/Sr	0.44	1.71	0.62	0.59	2.69	2.59	1.91	2.03	1.17
Nd/Th	1.51	1.72	1.35	0.31	0.54	1.12	1.07	1.16	1.60
Y+Nb	29.44	35.70	31.96	24.00	46.80	37.90	36.90	35.60	38.70

Note: XN6-7, XN18, XN23-1 are from Ma et al. (2016); 16LLMH1, 16LLMH2, 16LLMH3 are from Guo et al. (2019); Other samples are from this study.

10.3389/feart.2022.963351

(Figures 8C,D), and also many mafic rock units (Xin et al., 2019). In Yanshanian period, plate collision was close to the late stage, and the magmatism was mainly driven by crustal delamination in an extensional environment (Yang et al., 2010). The ore-bearing rocks in the East Kunlun Orogen were mainly formed in the Early-Middle Triassic subduction-continental collision stage (235–248 Ma), but a few of them were also formed in the Late Triassic post-collisional stage (204–219 Ma). For example, the Jiangjunmu ore-bearing granodiorite porphyry in the eastern East Kunlun was dated at 218 Ma (Yu et al., 2020), whilst the Huanglonggou granodiorite (also in eastern East Kunlun) was dated at 220 Ma (Zhang et al., 2017). In this study, emplacement of the ore-related Harizha granodiorite porphyry (217.3 ± 1.8 Ma) and granite porphyry (217.0 ± 1.7 Ma) was coeval with the post-collision stage in the East Kunlun Orogen (Gao et al., 2017). In addition, the samples plot in the volcanic arc-collisional granites field in the Nb-Y discrimination plot (Figure 12A) and in the post-collisional granites field in the Y+Nb-Rb discrimination plot (Figure 12B)), which also suggests that the Harizha granites were formed in a post-collisional extension environment (Han J. J. et al., 2020).

Data availability statement

The original contributions presented in the study are included in the article/supplementary material further inquiries can be directed to the corresponding author.

Author contributions

All authors contributed to the study conception and design. Material preparation, data collection and analysis were performed by WZ and CX. The first draft of the manuscript was written by WZ. CX, WZ, and ZH made field investigation and collected samples; SZ and CQ took part in the experiments; CX and WZ interpreted all the data and finished the original draft of the manuscript.

Funding

This study was supported by the Application Basic Research Project of Qinghai Science and Technology Plan (2020-ZJ-762).

Acknowledgments

We thank the Laboratory of the Hebei Institute of Regional Geology and Mineral Resources Survey, the State Key Laboratory of Continental Dynamics (Northwest University), and the Department of Geological Engineering (Qinghai University) for providing technical and platform support for the analyses in this study.

Conflict of interest

The authors declare that the research was conducted in the absence of any commercial or financial relationships that could be construed as a potential conflict of interest.

Publisher's note

References

Belousova, E. A., Kostitsyn, Y. A., Griffin, W. L., Begg, G. C., O'Reilly, S. Y., Pearson, N. J., et al. (2010). The growth of the continental crust: Constraints from zircon Hf-isotope data. *Lithos* (119), 457–466. doi:10.1016/j.lithos.2010.07.024

Chen, X. H., Yang, N., Chen, Z. L., Han, S. Q., Wang, Z. H., and Ye, B. Y. (2010). Geological characteristics and metallogenic model of super-large porphyry copper deposit in Aktogai ore field, Kazakhstan. *J. Geomechanics* 16 (4), 325–339. (in Chinese with English abstract). doi:10.3969/j.issn.1006-6616.2010.04.001

Du, Y. L., Jia, Q. Z., and Han, S. F. (2012). Mesozoic tectono-magmatic-mineralization and copper-gold polymetallic ore prospecting research in east Kunlun metallogenic belt in Qinghai. *Northwest. Geol.* 45 (4), 69–75. (in Chinese with English abstract).

Feng, Y. L., Yuan, W. M., Tian, Y. T., Feng, X., Hao, N. N., Zhang, L., et al. (2017). Preservation and exhumation history of the harizha-halongxiuma mining area in the east Kunlun range, northeastern Tibetan plateau, China. *Ore Geol. Rev.* 90, 1018–1031. doi:10.1016/j.oregeorev.2016.12.029

Frost, B. R., Barnes, C. G., Collins, W. J., Arculus, R. J., Ellis, D. J., Frost, C. D., et al. (2001). A geochemical classification for granitic rocks. *J. Petrology* 42 (11), 2033–2048. doi:10.1093/petrology/42.11.2033

Gao, H. C., and Sun, F. Y. (2001). Middle to late triassic granitic magmatism in the East Kunlun Orogenic Belt, NW China: Petrogenesis and implications for a transition from subduction to post-collision setting of the Palaeo-Tethys Ocean. *Geol. J.* 56 (6), 3378–3395. doi:10.1002/gj.4104

Gao, Y. B., Li, W. Y., Li, K., and Qian, B. (2017). Magmatism and mineralization during early mesozoic continental accretion process in qimantag, East Kunlun mountains. *Mineral. Deposits* 36 (2), 463–482. (in Chinese with English abstract). doi:10.16111/j.0258-7106.2017.02.013

Gibbs, A. K. (1986). *The continental crust: Its Composition and evolution*. Stuart ross taylor , scott M. McLennan. *J. Geol.* 94 (4), 632–633. doi:10.1086/629067

Griffin, W. L., Pearson, N. J., Belousova, E., Jackson, S. E., O'Reilly, S. Y., and Shee, S. R. (2000). The Hf isotope composition of cratonic mantle: LAM-MC-ICPMS analysis of zircon megacrysts in kimberlites. *Geochimica Cosmochimica Acta* 64 (1), 133–147. doi:10.1016/S0016-7037(99)00343-9

Guo, F. Z., and Deng, J. F. (1998). Late Paleozoic-Mesozoic intracontinental orogenic process and intermediate-acidic igneous rocks from the Eastern Kunlun Mountains of Northwestern China. *Geoscience* 12 (3), 344–352. (in Chinese with English abstract).

Guo, X. Z., Jia, Q. Z., Kong, H. L., Li, Y. Z., Li, J. C., and Wang, Y. (2016). Zircon U-Pb geochronology and geochemistry of Harizha quartz diorite in the eastern section from East Kunlun. *Geol. Sci. Technol. Inf.* 35 (5), 18–26. (in Chinese with English abstract). doi:10.3969/j.issn.0001-5717.2016.10.019

Guo, X. Z., Jia, Q. Z., Li, J. C., Kong, H. L., Yao, X. G., and Ma, Z. Y. (2019). The forming age and geochemistry characteristics of the granodiorites in Harizha, East Kunlun and its tectonic significance. *J. Geomechanics* 25 (2), 286–300. (in Chinese with English abstract). doi:10.12090/j.issn.1006-6616.2019.25.02.027

Han, J. J., Li, Y. D., Song, C. Z., He, J., Han, X., and He, X. L. (2020). Zircon U- Pb dating and geochemistry of granite in the Reshui area of Dulan County, eastern section of east Kunlun orogen and its tectonic implications. *Acta Geol. Sin.* 94 (3), 768–781. (in Chinese with English abstract).

Han, Z. H., Sun, F. Y., Tian, N., Gao, H. C., Li, L., and Zhao, T. F. (2020). Zircon U-Pb geochronology, geochemistry and geological implications of the early Paleozoic Wulanwuzhuer granites in the Qimantag, East Kunlun, China. *Earth Sci.*, 1–27. (in Chinese with English abstract).

Horn, I., Rudnick, R. L., and McDonough, W. F. (2000). Precise elemental and isotope ratio determination by simultaneous solution nebulization and laser ablation-ICP-MS: Application to U-Pb geochronology. *Chem. Geol.* 164, 281–301. doi:10.1016/S0009-2541(99)00168-0

Hoskin, P. W. O., and Schaltegger, U. (2003). The composition of zircon and igneous and metamorphic petrogenesis. *Rev. Mineralogy Geochem.* 53 (1), 27–62. doi:10.2113/0530027

Huang, D. M., Wan, Y. S., Zhang, D. H., Dong, C. Y., and Zhao, Y. Y. (2016). Paleoproterozoic tectono—thermal events in the xiatang area, lushan county, southern margin of the north China craton—evidence from geochemical features, zircon SHRIMP dating and Hf isotopic analysis. *Geol. Rev.* 62 (6), 1439–1461. doi:10.16509/j.georeview.2016.06.006

Karl, R. J., Eduardo, C., Jamie, J. W., Clara, C. W., Anton, K., Miranda-Diaz, G., et al. (2021). Hydrothermal fluid evolution in the Escondida porphyry copper deposit, northern Chile: Evidence from SEM-CL imaging of quartz veins and LA-ICP-MS of fluid inclusions. *Min. Depos.* 57, 279–300. doi:10.1007/S00126-021-01058-Z

Lei, Y., Shu, Y. D., Zhi, C. L., Zhao, C., Pang, Z., Yu, X., et al. (2020). Origin of the late permian gabbros and middle triassic granodiorites and their mafic microgranular enclaves from the eastern Kunlun orogen belt: Implications for the subduction of the palaeo-tethys ocean and continent-continent collision. *Geol. J.* 55 (1), 147–172. doi:10.1002/gj.3340

Li, H. P. (2010). *Metallogenic geological characteristics and Metallogenic prediction of Qimantage iron and polymetallic deposit of East Kunlun Mountains*, Doctoral Dissertation. Beijing): China University of Geosciences, 1–168.

Li, J. Q., Zhang, X. L., Wang, T., Li, Q., Wang, T. S., and Xue, W. W. (2021). Zircon U-Pb dating and geochemical characteristics of granite porphyry in Zhanhongshan area, East Kunlun. *Northwest. Geol.* 54 (1), 30–40. (in Chinese with English abstract). doi:10.19751/j.cnki.61-1149/p.2021.01.003

Li, Q. (2019). *Study on the Geological characteristics and enrichment regularities of mineralization of Harizha Ag-Cu polymetallic deposit in Eastern Kunlun orogenic belt, Qinghai Province*. Master Dissertation. Jilin: Jilin University, 1–80.

Li, X. R., Wan, Y. L., and Wang, J. (2020). Petrogeochemical characteristics, zircon U-Pb ages and Hf isotopic composition of Baicuo granites in central Qiangtang Basin, and its tectonic significance. *Geol. Rev.* 66 (5), 1172–1185. (in Chinese with English abstract). doi:10.16509/j.georeview.2020.05.007

Li, Y. J., Wei, J. H., Santosh, M., Li, H., Liu, H., Niu, M., et al. (2020). Anisian granodiorites and mafic microgranular enclaves in the eastern Kunlun Orogen, NW China: Insights into closure of the eastern Paleo-Tethys. *Geol. J.* 55 (9), 6487–6507. doi:10.1002/gj.3814

Liu, B., Ma, C. Q., Jiang, H. A., Guo, P., Zhang, J. Y., and Xiong, F. H. (2013). Early Paleozoic tectonic transition from ocean subduction to collisional orogeny in the Eastern Kunlun region: Evidence from Huxiaoqin mafic rocks. *Acta Petrol. Sin.* 29 (6), 2093–2106. (in Chinese with English abstract).

Liu, J., Huang, B., Yang, T., Xu, W. J., Liu, M., and Cao, Q. C. (2019). Analysis on the super-large porphyry copper deposits in the world. *Geol. Resour.* 28 (4), 345–349+400. (in Chinese with English abstract). doi:10.13686/j.cnki.dzyzy.2019.04.006

Lv, P. R., Yao, W. G., Zhang, H. D., Tian, H. H., and Yang, B. (2017). Geological characteristics of the Saindak porphyry Cu-Au deposit in Pakistan and its main ore-controlling factor. *Geol. Sci. Technol. Inf.* 36 (2), 206–214. doi:10.19509/j.cnki.dzkq.2017.0227

Ma, Z. Y., Li, L. J., Zhou, Q. L., Ma, C. X., and Zhao, J. P. (2013). The characteristics of the porphyry copper deposit and its formation in the East Kunlun Harizha area. *J. Qinghai Univ. Nat. Sci. Ed.* 31 (3), 69–75. (in Chinese with English abstract). doi:10.13901/j.cnki.qhwxxbzk.2013.03.012

Ma, Z. Y., Sun, F. F., Hao, N. N., Ma, C. X., Zhu, C. B., and Cao, J. H. (2016). Geochemical characteristics and metallogenic environment of granite in the Harizha copper polymetallic deposit area, Qinghai. *Mineral. Explor.* 7 (6), 929–937. (in Chinese with English abstract). doi:10.3969/j.issn.1674-7801.2016.06.006

Maniar, P. D., and Piccoli, P. M. (1989). Tectonic discrimination of granitoids. *Geol. Soc. Am. Bull.* 101 (5), 635–643. doi:10.1130/0016-7606(1989)101<0635:tdog>2.3.co;2

McDonough, W. F., and Sun, S. S. (1995). The composition of the Earth. *Chem. Geol.* 120 (3/4), 223–253. doi:10.1016/0009-2541(94)00140-4

Middlemost, E. A. K. (1985). *Magmas and magmatic rocks*. London: Longman, 1–266.

Pan, G. T., Xiao, Q. H., Lu, S. N., Deng, J. F., Feng, Y. M., and Feng, Y. F. (2009). Subdivision of tectonic units in China. *Geol. China* 36 (1), 1. 16+255+17-28. (in Chinese with English abstract).

Park, J. W., Campbell, I. H., Chiaradia, M., Hao, H. D., and Lee, C. T. (2021). Crustal magmatic controls on the formation of porphyry copper deposits. *Nat. Rev. Earth Environ.* 8 (2), 542–557. doi:10.1038/s43017-021-00182-8

Pearce, J. A., Harris, N. B. W., and Tindle, A. G. (1984). Trace element discrimination diagrams for the tectonic interpretation of granitic rocks. *J. Petrology* 25, 956–983. doi:10.1093/petrology/25.4.956

Qi, S. S. (2015). *Petrotectonic assemblages and tectonic evolution of the East Kunlun orogenic belt in Qinghai Province*. Doctoral Dissertation. Beijing: China University of Geosciences, 1–343.

Qian, Z. Z., Hu, Z. G., Liu, J. Q., and Li, H. M. (2000). Active continental margin and regional metallogenesis of the paleo-tethys in the east Kunlun mountains. *Geotect. Metallogenia* (2), 134–139.

Rudnick, R., , and Gao, S. (2004). *Treatise on geochemistry*. Elsevier Science, Holland and Turekian Composition of the Continental Crust3, 1–64.

Shao, F. L., Niu, Y. L., Liu, Y., Chen, S., Kong, J. J., Duan, M., et al. (2017). Petrogenesis of triassic granitoids in the east Kunlun orogenic belt, northern Tibetan plateau and their tectonic implications. *Lithos* 282, 33–44. doi:10.1016/j.lithos.2017.03.002

Song, B. Z., Zhang, Y. L., Chen, X. Y., Jiang, L., Li, D. S., and Kong, H. L. (2013). Geochemical characteristics of Harizha granite diorite-porphyry in East Kunlun and their geological implications. *Mineral. Deposits* 32 (1), 157–168. (in Chinese with English abstract). doi:10.3969/j.issn.0258-7106.2013.01.011

Sun, F. F., Zhu, C. B., Yuan, W. M., Zhang, A. K., Ma, Z. Y., and Feng, Y. L. (2016). Apatite fission track analysis of tectonic activity in Harizha polymetallic ore district, Dulan county, Qinghai province. *Nucl. Tech.* 39 (12), 41–48. (in Chinese with English abstract). doi:10.11889/j.0253-3219.2016.hjs.39.120501

Sun, S. S., and McDonough, W. F. (1989). "Chemical and isotopic systematics of oceanic basalts: Implications for mantle composition and processes,". Editors A. D. Saunders, and M. J. Norry (Geological Society London Special Publications), 42, 313–345.*Magmatism ocean basins*. doi:10.1144/gsl.sp.1989.042.01.19

Sun, X., Hollings, P., and Lu, Y. J. (2021). Geology and origin of the Zhunuo porphyry copper deposit, Gangdese belt, southern Tibet. *Min. Depos.* 3 (56), 457–480. doi:10.1007/s00126-020-00970-0

Sylvester, P. J. (1998). Post-collisional strongly peraluminous granites. *Lithos* 45 (1/4), 29–44. doi:10.1016/S0024-4937(98)00024-3

Tang, J. X., Wang, D. H., Wang, X. W., Zhong, K. H., Ying, L. J., and Tang, X. Q. (2010). Geological features and metallogenic model of the jiama copper-polymetallic deposit in Tibet. *Acta Geosci. Sin.* 31 (4), 495–506.

Urqueta, E., Kurt, K. T., Clark, A. H., Stanley, C. R., and Oates, C. J. (2009). Lithogeochemistry of the Collahuasi porphyry Cu–Mo and epithermal Cu–Ag (–Au) cluster, northern Chile: Pearce element ratio vectors to ore. *Geochem. Explor. Environ. Anal.* 9 (1), 9–17. doi:10.1144/1467-7873/07-169

Wang, G. (2014). *Metallogenesis of nickel deposits in eastern Kunlun orogenic belt, Qinghai Province. Doctoral dissertation*. Jilin: Jilin University, 1–214.

Wang, G., Sun, F. Y., Li, B. L., Li, S. J., Zhao, J. W., and Yang, Q. A. (2014). Petrography, zircon U-Pb geochronology and geochemistry of the mafic-ultramafic intrusion in Xiarihamu Cu-Ni deposit from East Kunlun, with implications for geodynamic setting. *Earth Sci. Front.* 21 (6), 381–401. (in Chinese with English abstract). doi:10.13745/j.esf.2014.06.036

Wang, K., Wang, L. X., Ma, C. Q., Zhu, Y. X., and Gao, L. Y. (2020). Petrogenesis and geological implications of the middle Triassic garnet-bearing two-mica granite

from Jialuhe Region, East Kunlun. *Earth Sci.* 45 (2), 400–418. (in Chinese with English abstract). doi:10.3799/dqkx.2018.393

Wang, P. X., Guo, F., and Wang, Z. N. (2020). Zircon U-Pb geochronology, geochemistry and geological significance of granitoids in the Yazigou, Qimantage area of East Kunlun Mountains. *Geoscience*, 1–14. (in Chinese with English abstract). doi:10.19657/j.geoscience.1000-8527.2020.026

Wang, X. L., Yuan, W. M., Feng, X., Feng, Y. L., and Cheng, X. Q. (2017). LA-ICP-MS zircon U-Pb age and geological significance of granite porphyry and diorite in the Harizha polymetallic ore district, East Kunlun Mountains. *Geol. Bull. China* 36 (7), 1158–1168.

Wu, D. Q., Sun, F. Y., Pan, Z. C., and Tian, Nan. (2020). Geochronology, geochemistry, and Hf isotopic compositions of triassic igneous rocks in the easternmost segment of the east Kunlun orogenic belt, NW China: Implications for magmatism and tectonic evolution. *Int. Geol. Rev.* 63, 1011–1029. doi:10.1080/00206814.2020.1740895

Wu, F. Y., Li, X. H., Zheng, Y. F., and Gao, S. (2007). Lu-Hf isotopic systematics and their applications in petrology. *A cta Petrol. Sin.* 23 (02), 185–220. doi:10.3321/j.issn:1000-0569.2007.02.001

Xia, C. L. (2018). *Research on the copper-lead-zinc-silver polymetallic metallogenic system related to magma-volcano hydrothermal in the eastern part of East Kunlun*, Doctoral Dissertation. Beijing: China University of Geosciences, 1–174.

Xia, R., Wang, C. M., Deng, J., Carranza, E. J. M., Li, W. L., Qing, M., et al. (2014). Crustal thickening prior to 220 Ma in the east Kunlun orogenic belt: Insights from the late triassic granitoids in the xiao-nuomuhong pluton. *J. Asian Earth Sci.* 93, 193–210. doi:10.1016/j.jseaes.2014.07.013

Xiao, Q. H., Deng, J. F., and Ma, D. Q. (2002). *Thinking and method of granite research*. Beijing: Geological Publishing House, 1–294.

Xin, W., Sun, F. Y., Zhang, Y. T., Fan, X. Z., Wang, Y. C., Li, L., et al. (2019). Mafic–intermediate igneous rocks in the East Kunlun Orogenic Belt, northwestern China: Petrogenesis and implications for regional geodynamic evolution during the Triassic. *Lithos* 346-347, 105159. doi:10.1016/j.lithos.2019.105159

Xu, B., Wang, C. Y., Liu, J. D., Wei, L. Q., Ji, M. J., and Li, X. (2020). The petrogenesis of the late triassic granites heergetou area, East Kunlun: Constraints from geochronology, geochemistry and Sr-Nd-Pb isotopes. *Acta Geol. Sin.* 94 (12), 3643–3656. (in Chinese with English abstract). doi:10.19762/j.cnki.dizhixuebao.2020284

Xu, X. B., Wang, L. X., Ma, C. Q., Zhu, Y. X., and Wang, K. (2021). Petrogenesis and geological implications of the yangfengou intermediate-felsic dykes in the balong area within the eastern Kunlun orogen. *Bull. Mineralogy, Petrology Geochem.*, 1–24. (in Chinese with English abstract). doi:10.19658/j.issn.1007-2802.2021.40.021

Yan, Z. J. (2019). *Genesis of silver polymetallic deposit in Harizha area Qinghai Province. Master dissertation*. Jilin: Jilin University, 1–62.

Yang, H. Y., Ma, W. M., and Wang, G. Z. (2015). The prospecting sign of copper polymetallic deposit in Harizha area, Qinghai. *Mod. Min.* 31 (10), 140–143. (in Chinese with English abstract). doi:10.3969/j.issn.1674-6082.2015.10.045

Yang, P., Pei, S. J., Chen, L. J., Tang, J., and Zhao, H. X. (2010). Characteristic of copper-bearing porphyry and analysis on the Prospecting potential in Harizha of Qinghai. *J. Qinghai Univ. Nat. Sci.* 28 (06), 62–68. (in Chinese with English abstract). doi:10.13901/j.cnki.qhwxxbzk.2010.06.009

Yang, T., Zhou, H. B., Zheng, Z. H., Liu, H., Li, J., Li, M. T., and Wang, Y. (2017). Geological characteristics and genetic type of the Nagengkangqieer silver polymetallic deposit in East Kunlun. *Northwest. Geol.* 50 (04), 186–199. (in Chinese with English abstract). doi:10.19751/j.cnki.61-1149/p.2017.04.020

Yang, Z. L., Hu, X. J., Wang, S. Q., Xin, H. T., Li, C. D., Liu, W. G., et al. (2020). Geochronology, geochemistry and geological significance of early paleozoic volcanic rocks in northern east ujimqin banner, inner Mongolia. *Acta Petrol. Sin.* 36 (4), 1107–1126. (in Chinese with English abstract). doi:10.3969/j.issn.1000-8845.2006.02.021

Yao, W. G., Hong, J., Yang, B., and Lv, P. R. (2013). Types and characteristics of main copper deposits in Pakistan. *Acta Mineral. Sin.* 33 (S2), 1076–1077. (in Chinese with English abstract). doi:10.16461/j.cnki.1000-4734.2013.s2.092

Yu, J. Z., Zheng, Y. Y., Xu, R. K., Hou, W. D., and Cai, P. J. (2020). Zircon U-Pb chronology, geochemistry of Jiangjunmu ore-bearing pluton, eastern part of East Kunlun and their geological significance. *Earth Sci.* 45 (04), 1151–1167. (in Chinese with English abstract). doi:10.3799/dqkx.2019.134

Yuan, H. L., Wu, F. Y., Gao, S., Liu, X. M., Xu, P., and Sun, D. Y. (2003). Zircon laser probe U-Pb dating and REE composition analysis of Cenozoic intrusions in Northeast China. *Chin. Sci. Bull.* 48 (14), 1511–1520. (in Chinese with English abstract).

Zhong, M. F. (2018). *Discussion on the application of integrated geophysical methods in the exploration of the Harizha polymetallic ore in Dulan County, Qinghai Province*. Master Dissertation. Jilin: Jilin University, 1–57.

Zhai, Y. S., Yao, S. Z., and Cai, K. Q. (2011). *Mineral deposits*. Beijing: Geological Publishing House.

Zhang, B., Guo, F., and Zhang, X. B. (2020). Petrogenesis of granitic rocks in the Pingtan Island, Fujian Province: Constraints from zircon U▪Pb dating, O▪Hf isotopes and biotite mineral chemistry. *Acta Petrol. Sin.* 36 (4), 995–1014. doi:10.18654/1000-0569/2020.04.02

Zhang, B., Kong, H. L., Li, Z. M., Li, J. C., Yang, T., and Wang, Y. (2016). Zircon U-Pb dating, geochemical and geological significance of the tonalites from the Harizha lead-zinc polymetallic mine in East Kunlun Mountains. *Geol. Sci. Technol. Inf.* 35 (5), 9–17. (in Chinese with English abstract).

Zhang, J. Y., Ma, C. Q., Li, J. W., and Pan, Y. M. (2017). A possible genetic relationship between orogenic gold mineralization and postcollisional magmatism in the eastern Kunlun Orogen, Western China. *Ore Geol. Rev.* 81, 342–357. doi:10.1016/j.oregeorev.2016.11.003

Zhang, Z. W., Wang, Y. L., Wang, C. Y., Qian, B., Li, W. Y., Zhang, J. W., et al. (2019). Mafic-ultramafic magma activity and metallogeny during paleozoic in the eastern Kunlun orogenic belt, Qinghai province, China. *China Geol.* 2 (4), 1–11. doi:10.31035/cg2018124

Zhou, H. Z., Zhang, D. H., Wei, J. H., Wang, D. Z., Santosh, M., Shi, W. J., et al. (2020). Petrogenesis of Late Triassic mafic enclaves and host granodiorite in the Eastern Kunlun Orogenic Belt, China: Implications for the reworking of juvenile crust by delamination-induced asthenosphere upwelling. *Gondwana Res.* 84, 52–70. doi:10.1016/j.gr.2020.02.012